CONVERSION OF PRECERAMIC POLYMER BRUSHES AND BRUSH COMPLEXES TO CERAMIC BY LASER ANNEALING ON SILICON WAFERS AND SILICA NANOPARTICLES

A Thesis

Presented to the Faculty of the Graduate School

of Cornell University

In Partial Fulfillment of the Requirements for the Degree of

Master of Science

by

Ishwari Chaitanya Joshi

August 2025

ABSTRACT

Thermally stable materials are necessary for high-performance ceramic coatings, but traditional annealing techniques can be laborious and slow. This study investigates the use of laser annealing to quickly transform brush-functionalized silica nanoparticles and preceramic polymer brushes into ceramics.

The Stöber process was used to create silica nanoparticles, which were then functionalized for polymerization. SiC brushes were made from 3-(1,1,1,5,5,5-hexamethyl-3-((trimethylsilyl)oxy)trisiloxan-3-yl)propyl methacrylate, and SiN brushes were made from PDMAEMA complexed with Durazane 1800. Polymer brushes were grafted onto silicon substrates using ATRP. By using emulsion polymerization, core-shell silica nanoparticles with SiC shells were created.

Rapid polymer-to-ceramic conversion was made possible by laser annealing, creating thermally stable SiC_xN_y. materials. For applications involving nanocomposite materials and sophisticated ceramic coatings, this method provides an effective substitute.

BIOGRAPHICAL SKETCH

Ishwari Chaitanya Joshi, born on September 15, 2001, in India, completed her schooling at Balmohan Vidyamandir in Mumbai. She went on to complete her bachelor's degree in Fibers and Textiles Processing Technology at the Institute of Chemical Technology, Mumbai. During her undergraduate degree, she developed passion for research in the realm of fibers and polymers. This interest led her to pursue a Master of Science degree at Cornell University, where she worked in the field of polymers under the guidance of Professor Christopher Ober.

ACKNOWLEDGMENTS

First and foremost, I would like to express my deepest gratitude to my advisor, Prof. Christopher Ober, for his invaluable guidance, encouragement, and unwavering support throughout the course of this research. His insights and feedback consistently pushed me to improve and expand my understanding. I would also like to thank my mentor, Dr. Yu Shao, who taught me everything I know about research. My time under his mentorship will always be cherished and looked back upon fondly.

I would also like to extend my heartfelt gratitude to Professor David B. Zax, Director of the M.S. Graduate Program in Chemistry and Chemical Biology. He accepted me into the program and showed immense faith in me. His belief in my potential has been a cornerstone of my graduate experience, and I will carry his mentorship with me always.

Additionally, I would extend my gratitude towards all the Ober group lab members, including, Gozde and Madan, who helped me in times of crisis and guided me towards solutions. I would like to credit and thank Abhishek Kulkarni and Haelin Park for helping with parts of my experiment.

I would like to thank my brother, Vrushaank, for being my closest confidant, my sister, Ishanee, for being there when no one else was and my late grandfather, who I hope would be proud of me.

I would also like to extend my gratitude towards my aunt, Roma and my cousin Ronav, who have been my constant supporters through this journey. To my friends- Stuti, Sahil, Khetal, Shubham, Shikhar, Bhavika and AJ, thank you for being my anchors through it all. I am truly grateful for your presence and love.

Lastly, I would like to thank my parents, for always pushing me to do what's best for me, even if that meant having to make hard decisions. I hope that I have been able to make you both proud and I hope you know that your love will always be the foundation beneath every accomplishment.

TABLE OF CONTENTS

LIST OF FIGURES

LIST OF TABLES

LIST OF ABBREVIATIONS

AFM Atomic Force Microscopy

AIBN 2,2′-azobisisobutyronitrile

APTES 3-Aminopropyltriethoxysilane

ARGET-ATRP Activators ReGenerated by Electron Transfer Atom Transfer Radical Polymerization

BIBB 2-Bromoisobutyryl bromide

CMC Ceramic Matrix Composites

DCM Dicholormethane

DLS Dynamic light scattering

DMAEMA 2-dimethylaminoethyl methacrylate

DMF Dimethylformamide

DMSO Dimethyl sulfoxide

EDX Energy-dispersive X-ray

FRP Free Radical Polymerization

MMC Metal Matrix Composites

MPS 3-(trimethoxysilyl)propyl methacrylate

PCPs Preceramic Polymers

PCS Polycarbosilane

PDCs Polymer-Derived Ceramics

PDMAEMA Poly(dimethylaminoethyl methacrylate)

PMC Polymer Matrix Composites

SDS Sodium dodecyl sulfate

SEM Scanning Electron Microscopy

SI-ATRP Surface-Initiated Atom Transfer Radical Polymerization

TEA Triethylamine

TEM Transmission Electron Microscopy

TEOS Tetraorthosilicate

THF Tetrahydrofuran

XPS X-ray Photoelectron Spectroscopy

CHAPTER 1: INTRODUCTION

1.1 Introduction

In 1903, the Wright Brothers built the world's first plane – the Wright Flyer. This was a basic structure that was made out of wood, fabric and metal (Jakab, 1997). Since then, modern aircraft have seen significant changes to their structure, making them more resilient, being able to reach greater heights and speeds and withstand turbulence and other severe weather conditions. To make modern aircraft, alloys or superalloys made from aluminum, titanium, iron, cobalt, nickel and other metals have been used in the past. Composite materials have also seen an uptake in usage as 25% of the Airbus A380 and 50% of the Boeing 787 aircraft are made from these materials. These include ceramic matrix composites (CMC), metal matrix composites (MMC) and polymer matrix composites (PMC) (S. Zhang & Zhao, 2012; X. Zhang et al., 2018). They may include matrices such as silicon carbide (SiC) and silicon nitride (Si_3N_4).

Of all these materials, ceramics have shown great promise in the material science world. Ceramics must be able to withstand high temperatures and mechanical stress to be useful in aircraft. This is important in aircraft due to their jet engines operating above 1700^{o}C (Feigenoff, Charlie, 2018) and their general wear and tear makes it necessary to have materials that are able to endure high mechanical stress. Inherently, ceramics are known to be resistant to high temperatures but brittle by nature. To help solve this problem, the tunability of these ceramics becomes an important factor. Properties of ceramics can be tailored if they are made from preceramic polymers (PCPs). Polymer-derived ceramics (PDCs) are the ceramics formed through the heat treatment of PCPs (Packirisamy et al., 2020). PDCs are known to follow the concept of "better chemistry through ceramics". These preceramic polymers can be used to produce binary, ternary, quaternary or more complex ceramics (Mera & Ionescu, 2019). Such ceramics thus

formed from such preceramic polymers have the ability to withstand high temperatures and mechanical stress.

Polymer-derived ceramics were first recognized when Fritz and Raabe published their work on the thermal decomposition of organosilicon precursors to ceramics in 1956 (Fritz & Raabe, 1956). This was followed by Ainger and Herbert in 1960, who published their work on P—N nonporous solids derived from polyphosphazenes (Ainger & Herbert, 1960). In 1963, Weyer received his patent for his work on the preparation of ceramics from tailor-made precursors (Weyer, 1963). Soon after, Chantrell and Popper showed that monolithic silicon nitride could be made by forming polysilazane into the required shape and then pyrolyzing it, indicating that inorganic polymers could be extremely promising precursors for advanced ceramics. In Germany, in the 1970s Verbeek et al. reported pyrolyzing polysilazane and polycarbosilazane to create non-oxide ceramic fiber made of silicon carbide and silicon nitride (Verbeek, 1974). In Japan, Yajima and colleagues synthesized polycarbosilane (PCS) from polydimethylsilane and assessed it as a precursor for silicon carbide fiber (Yajima et al., 1976).

Silicon based ceramic precursors have been used for their applications in high temperature environments, specifically, SiC and Si_3N_4. These ceramics can endure temperatures within the range of 1600-1700°C (Kane et al., 2021). Moreover, Si_3N_4 and SiCN ceramics have many desirable mechanical properties, such as strength and hardness, along with the ability to withstand very high temperatures. A drawback of having these properties is that the firing conditions of these preceramics become unique. They may need to be cross-linked before pyrolysis and the firing temperatures need to be sufficiently high (Ackley et al., 2023). In the study done by A. Li et al., the addition of cross-linker dramatically increased the film-growth rate

(A. Li et al., 2011). This could help the brush improve its thickness and improve conversion rate from PCP to ceramic.

1.2 Polymerization and surface modification

Polymer brushes are special macromolecular structures with polymer chains densely tethered to a surface which could be planar or spherical via a stable covalent or noncovalent bond linkage (Feng & Huang, 2018). The polymer chains are congested and compelled to stretch away from the surface or interface to prevent overlapping since the tethering is so dense, often reaching considerably farther than a chain would normally extend when unstretched (Zhao & Brittain, 2000a). There are three methods for formation of these “tethered polymer chains” (Figure 1). The first one is physisorption, the selective adsorption of one block of a diblock copolymer to a surface (Brittain & Minko, 2007; Parsonage et al., 1991). Conversely, the covalent attachment of these polymer chains can be done in two ways- “grafting to” and “grafting from”. The "grafting to" technique creates tethered chains by reacting (end-)functionalized polymer molecules with corresponding functional groups on the surface. On the other hand, in the "grafting from" method, the attached initiating groups start a polymerization process at the substrate surface (Zdyrko & Luzinov, 2011).

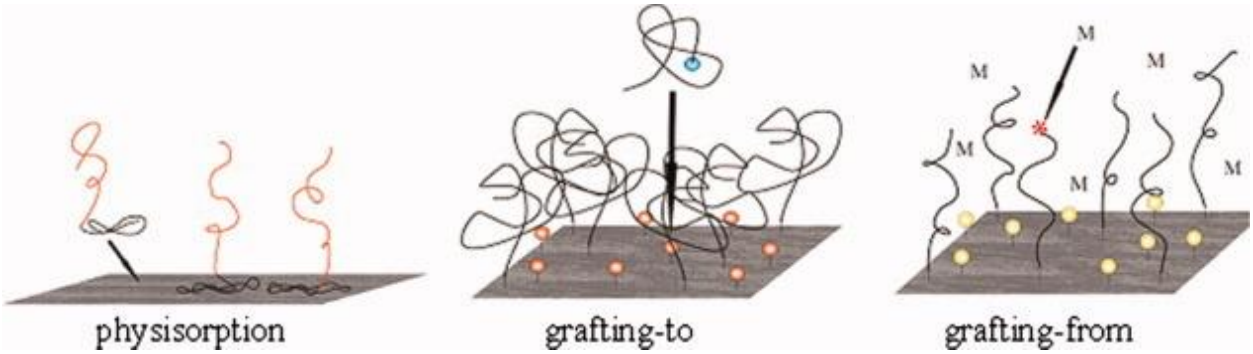

Figure 1. 1: Methods of polymer brush formation (Brittain & Minko, 2007).

While most polymer brushes are synthesized from styrene or methacrylate monomers, PCPs can also be modified to produce brushes of tailored molecular weight, narrow dispersity and controlled composition and architecture. An example of a preceramic polymer brush would be what was done by Park et al. Park et. al developed a preceramic polymer route to Cr-doped forsterite (Park et al., 1994).

To grow polymer brushes, a technique called surface-initiated (SI) living polymerization can be used. Surface-initiated Atom Transfer Radical Polymerization (SI-ATRP) has been used in the past to grow polymer brushes from metal sulfides, metal oxides and metal nanoparticles (Esteves et al., 2007; Khabibullin et al., 2016; Kurzhals et al., 2015; Vestal & Zhang, 2002). ATRP is a member of the reversible termination class of living polymerizations. They get their name because a reversible termination event, in which the chain-end is switched between an active and dormant species, regulates the chain's growth (Schork et al., 2005). This type of work was first demonstrated by Matyjaszewski et al, where they used ATRP to control polymer chain growth (Matyjaszewski & Xia, 2001; Qiu & Matyjaszewski, 1997; Wang & Matyjaszewski, 1995). Block copolymers, polymer brushes, and other complex structures can be synthesized with this

technique, which also provides remarkable control over the distribution of molecular weight. But, SI-ATRP has some disadvantages. It is an oxygen-sensitive process as the radicals generated can be quenched by the oxygen. It also requires high concentrations of transition metal catalysts.

To deal with the issues that occur during SI-ATRP, ARGET-ATRP can be used for polymer brush growth. ARGET-ATRP (Activators ReGenerated by Electron Transfer) is known for its ease of control of polymer brush growth, lack of oxygen sensitivity and requirement of only catalytic amounts of transition metals complexes (Bombalski et al., 2007; Szczepaniak et al., 2021). For the polymer-grafted nanoparticles, mini-emulsion techniques may be used for the ARGET-ATRP emulsion polymerizations. Mini-emulsion polymerization involves the use of an effective surfactant/costabilizer system to produce very small (0.01–0.5 mm) monomer micelle (Schork et al., 2005). This kind of polymerization may give high yield, controlled growth and narrow dispersity. The use of this technique can be observed in the work done by Yuan et. al (Yuan et al., 2022).

Emulsion polymerization may also be used for free radical polymerization. When unsaturated monomers undergo chain polymerization involving free radicals as a chain carrier, the process is referred to as “free-radical addition polymerization”(Yamada, 2015). Some Si-based ceramic precursors may be used as the monomers for polymerization. Some examples of these precursors are given in Figure 1.2. An initiator, such as AIBN, for example will help initiate the polymerization of the monomer. The radicals generated would be part of the emulsion system and will help carry forward the reaction until the termination occurs.

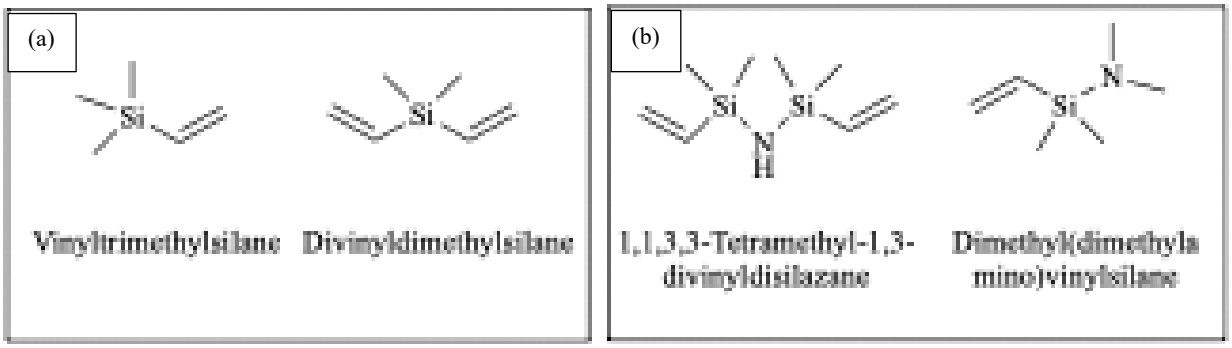

Figure 1. 2: Examples of ceramic precursors **(a):** SiC precursors; **(b):** Si3N4 precursors.

An important aspect of polymer-grafted nanoparticles is the nanoparticle itself. Nanoparticles may also be known as the core when describing inorganic-inorganic core shell structures. To carry out polymer growth on any type of nanoparticles, it is essential to functionalize them in a way that brush growth can take place, as mentioned previously. Silica nanoparticles are known for their simple synthesis, inexpensive nature, abundant yield and ability to functionalize their surface (A. Nayl et al., 2022; Kankala et al., 2020; L. Li et al., 2019).

A well-known method to functionalize silica is using 3-aminopropyltriethoxysilane (APTES) to form amine bonds on a surface. On reaction with an initiator like 2-bromoisobutyryl bromide (BIBB), the amines form amide linkages, leaving bromine groups on the surface to react with the monomer. This method needs to be carried out in the presence of triethylamine (TEA), a base, to react with the HBr formed during the APTES and BIBB reaction.

1.3 Laser annealing

The final step of converting a preceramic polymer to a ceramic is using high temperatures for the conversion. Generally, to set PCPs, high temperature furnace annealing is used. The atmospheric

conditions can also be varied to change the chemical composition of the ceramic. From the work done by Vaahs et. al, pure Si_3N_4 was produced by pyrolyzing the polymer in an ammonia environment, which eliminated practically all of the carbon from the PDC. On the other hand, the polymer was converted to SiCN rather than Si_3N_4 by pyrolysis in a nitrogen atmosphere (Song et al., 1994; Vaahs et al., 1992). This kind of atmosphere can be used to create nitride ceramics. Semiconductors are widely processed using laser spike annealing (Blum et al., 1989; Bowen et al., 2020; Jacobs et al., 2015; Jiang et al., 2013; Jung et al., 2010, 2011, 2012, 2014; Lécuyer et al., 2007; Lovell & Schork, 2020; Sha et al., 2009; S. H. Yu et al., 1995). Lasers can be a quick and effective way to set these kinds of polymers due to their ability to reach high temperatures in a short span of time. Polymers can withstand high temperatures of ~500 ^oC without the threat of degradation so long as the heat treatment lasts for a few milliseconds. Laser spike annealing can make the use of this concept as proven by Jung et. al (Jung et al., 2010).

CHAPTER 2: CONVERSION OF PRECERAMIC POLYMER BRUSHES AND BRUSH COMPLEXES TO A CERAMIC BY LASER ANNELING ON SILICON WAFERS

2.1 Introduction

A silicon wafer's uniformity, well-defined surface chemistry, and compatibility with a range of surface modification techniques make them popular substrates for producing polymer brushes. Reactive hydroxyl (-OH) groups found in silicon's native oxide layer allow for strong surface-initiated polymerization using silane coupling agents or other grafting methods (Zhao & Brittain, 2000b). Furthermore, silicon wafers are suited for processing conditions like annealing or laser treatment because of their exceptional mechanical and thermal stability (Bell, 1979; Narayan et al., 1978). The smooth surface of silicon wafers simplifies studies on polymer brush thickness, morphology, and uniformity. This enables the use of methods like Atomic Force Microscopy (AFM) and X-Ray Photoelectron Spectroscopy (XPS) (Jakša et al., 2013) that work well on planar surfaces. Keeping all these aspects in mind, silicon wafers can be used as a starting point to grow polymer brushes. The brushes thus formed will be more homogeneous, making it easier to replicate this work on 3D structures such as nanoparticles, with a proof of concept in mind.

In the work done by Tait et al., 2-dimethylaminoethyl methacrylate (DMAEMA) was used as the preceramic polymer. DMAEMA is a good PCP due to the availability of hydrogen bonding. If the surface functionalization allows for it, this can prove to be very useful. Similarly, a SiC precursor such as 3-(1,1,1,5,5,5-Hexamethyl-3-((trimethylsilyl)oxy)trisiloxan-3-yl)propyl methacrylate could also be used. As mentioned previously, a functionalization that allows for hydroxyl groups, such as the one obtained by treatment with APTES and BIBB could be a convenient starting point as shown in Figure 2.1.

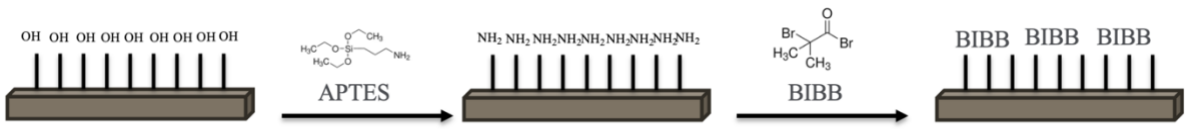

Figure 2. 1: Surface functionalization of silicon wafers.

The thermal treatment of preceramic polymers can be done using various methods such as using a tube furnace or laser spike annealing. It is also a good practice to cure the PCPs using temperatures within the ranges of 200-300^{o}C, in inert atmospheres. This may prevent further degradation of the PCPs due to contact with higher temperatures (~700 to 1300^{o}C during annealing) for extended periods of time, when fully setting them to ceramics in various atmospheres. In this manner, the PCPs grown on silicon wafers can be converted to ceramics.

This study investigates the synthesis, modification, and laser-assisted ceramic conversion of polymer brushes on silicon wafers to create thermally robust SiC_xN_y structures. Two types of polymer brushes were created based on PDMAEMA and a SiC monomer by functionalizing the wafer surfaces and employing surface-initiated polymerization. Attempts for cross-linking the SiC precursor have also been made. Characterization tools such as ellipsometry, Scanning Electron Microscopy (SEM), Atomic Force Microscopy (AFM), and X-ray Photoelectron Spectroscopy (XPS) are employed to assess brush morphology, thickness, and elemental composition before and after laser annealing. The experiments explain the transformation of these brushes under different annealing atmospheres (N_2 for SiN, NH_3 for SiC), and subsequent analysis, using XPS (Seah, 1980), confirms the incorporation of nitrogen. This enables us to replicate these studies on nanoparticle surfaces.

2.2 Experimental section

Preparation of silicon wafers: Silicon wafers were cut into 2 × 2 cm^2 or 1.5 x 2 cm^2 pieces and treated with Piranha solution (3 parts H_2SO_4+ 1-part H_2O_2) for 2 hours at room temperature. The wafers were then washed with de-ionized water and blow dried with nitrogen. The cleaned wafers were then set in the oven at 120^oC for a hot dry step for 1 hour. After this, the cleaned and dried wafers were allowed to soak in APTES 4% volume in ethanol for 1 hour followed by washing with ethanol and acetone. The APTES treated wafers were dried again in the oven at 120^oC for 30 minutes. These APTES treated, dried wafers were immersed in solution of BIBB (3 mmol) and TEA (3 mmol) in 15 mL DCM. The treated wafers with BIBB functionalization were taken out after 24 hours and then the polymer brushes were grown on the treated, BIBB functionalized wafers (Aktas Eken & Ober, 2022).

PDMAEMA brush growth: A solution of 3 mL monomer (PDMAMAE), 0.033 mL ligand (N,N,N',N',N"-pentamethyldiethylentriamine), 3 mL DMSO, 0.15 mL DI water was prepared. The treated wafers were placed in a petri dish, then submerged in the prepared solution and a copper plate was placed on top. The wafers were allowed to react for 2-3 hours, then taken out, washed with DMF and nitrogen blow dried.

PDMAEMA brush complexation and curing: In an inert environment, 5 weight % durazane in anhydrous toluene solution was prepared. The PDMAEMA brush wafers were soaked in this solution for 48 hours. After treatment, the brushes were taken out and washed with anhydrous toluene. The wafers with the polymer brushes formed complexes with the durazane. These

complexed wafers were cured using a continuous stream of nitrogen gas at 200^{o}C for 2 hours. Using this method, a silicon nitrile precursor brush (SiNPB) on surface can be achieved in principle (Tait et al., 2021).

SiC precursor brush growth: A solution of 3 mL monomer (3-(1,1,1,5,5,5-hexamethyl-3-((trimethylsilyl)oxy)trisiloxane-3-yl)propyl methacrylate), 0.033 mL ligand(N,N,N',N',N"-pentamethyldiethylentriamine), 3 mL anhydrous THF was prepared. The treated wafers were placed in a petri dish, then submerged in the prepared solution and a copper plate was placed on top. The wafers were allowed to react for 3-4 hours, then taken out of the reaction mixture, washed with anhydrous THF and nitrogen blow dried (see Figure 2.2).

SiC brush cross-linking: 10% by volume of allyl methacrylate was added to the solution prepared earlier. The previous steps were then repeated, the wafers placed at the bottom of their container, a new solution with cross-linker added was poured on top and then the copper plate was placed on top. Using this method, a silicon carbide precursor brush (SiCPB) on surface can be achieved in principle.

Addition of spacer: For the SiC brush, a silicon wafer piece that measured 2 × 0.5 cm^2 was placed on top of the APTES+BIBB treated wafer in a petri dish. These two were then submerged in the solution used for the SiC precursor brush growth and the copper plate was placed on top. Figure 2.2 shows the schematic for the same.

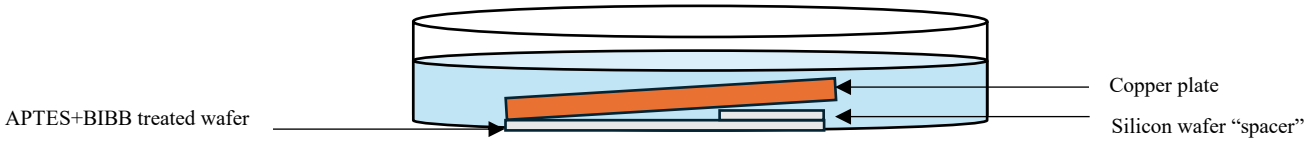

Figure 2. 2: Spacer schematic showing the method in which polymer brush growth took place, by placing spacer on top of treated wafer and finally placing the copper plate at an angle.

Laser annealing: The PDMAEMA brushes were annealed in a N_2 environment at, 750, 800 and 860ºC. The SiC brushes were annealed at 1209-1323ºC in an NH_3 environment.

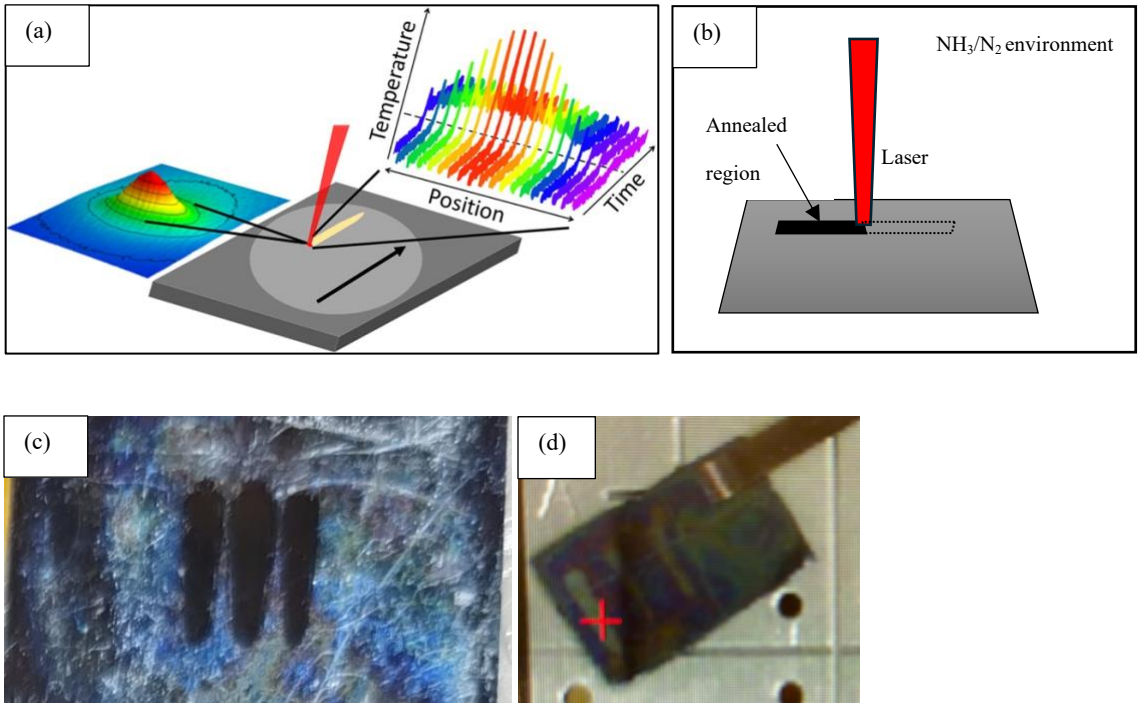

Figure 2. 3 (a): Laser spike annealing, **(b):** laser schematic, **(c):** SiC brush annealed using varying temperatures (1209-1323ºC left to right) and **(d):** PDMAEMA brush annealed using varying temperatures (left = 860ºC, middle = 750ºC, right = 800ºC).

Material characterization

The SiNPB and SiCPB were characterized using a Zeiss Gemini 500 **Scanning Electron Microscope** to observe how the surface of the wafers looked after brush growth. Samples were sputter-coated with gold for SEM analyses. The accelerating voltages used were 1 kV for the precomplexed and 5 kV for the complexed brushes respectively.

Ellipsometry results were obtained using the Woollam RC2 Spectroscopic Ellipsometer at the default settings to check the thickness of the PDMAEMA brushes. The Cauchy function was used to do the fittings.

For SiNPB, before and after complexation, film thickness grows from 200 nm to 300 nm.

For SiCPB, film thickness remains 60~100 nm.

The ellipsometry results were obtained for the PDMAEMA brushes and they are tabulated in table 2.1.

Sr. no.	Treatment time (in hours)	Brush thickness (in nm)
1	1	78
2	3	92
3	4	130

Table 2.1: PDMAEMA brush thickness measurements.

Atomic Force Microscopy was used to track the roughness of the polymer brush grown using the spacer. The equipment used was the Asylum-MFP3D-Bio-AFM-SPM. The probes used for the AFM were either the Olympus AC160TS-R3 or the AppNano ACCESS-NC tapping mode

probes. The scan size was 10 μm with a scan rate of 1 Hz. Imaging was conducted in tapping mode.

Profilometry was done using the Tencor AlphaStep 500 Profilometer. The height of the polymer brush was observed by creating a scratch on the spacer brush, as shown in Fig 2.4. The region observed was the yellowish part on the polymer brush grown using the spacer. The height difference was observed from the inside of the scratch (assuming that to be the lowest point) to the average height of the brush. The length it ran across was 5 mm.

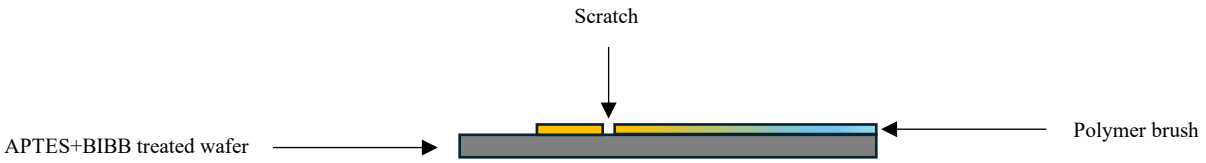

Figure 2. 4: Scratched brush schematic showing the transition between yellow (thick and uniform region) to blue (thin and non-uniform region).

X-ray Photoelectron Spectroscopy was done to tell the chemical composition of the brushes. The equipment used was the Thermo Scientific Nexsa G2 XPS. The X-ray spot size was 200 micrometers in diameter. Survery spectra was collected with a pass energy of 200 eV and a step size of 1 eV, and high resolution (> 5 scans) ones were collected with a pass energy of 50 eV and a step size of 0.1 eV. The carbon spectra were captured using 5 scans, the silicon spectra were captured using 10 scans, the nitrogen spectra were captured using 30 scans and the oxygen spectra were captured using 5 scans. Casa XPS software was used for data processing and Origin Pro was used to replot binding energy plots.

2.3 Results and Discussion

Scanning Electron Microscopy: From the SEM images of the SiNPB, the precomplexed and the complexed and cured wafers seemed to have different surface morphologies. Also, the EDX report as shown in Fig 2.7. showed the elemental difference between the precomplexed (labelled no nitrogen) and complexed (with durazane) and cured (labelled nitrogen) wafers. From the EDX, we could tell that the complexed and cured wafers had more nitrogen and more carbon.

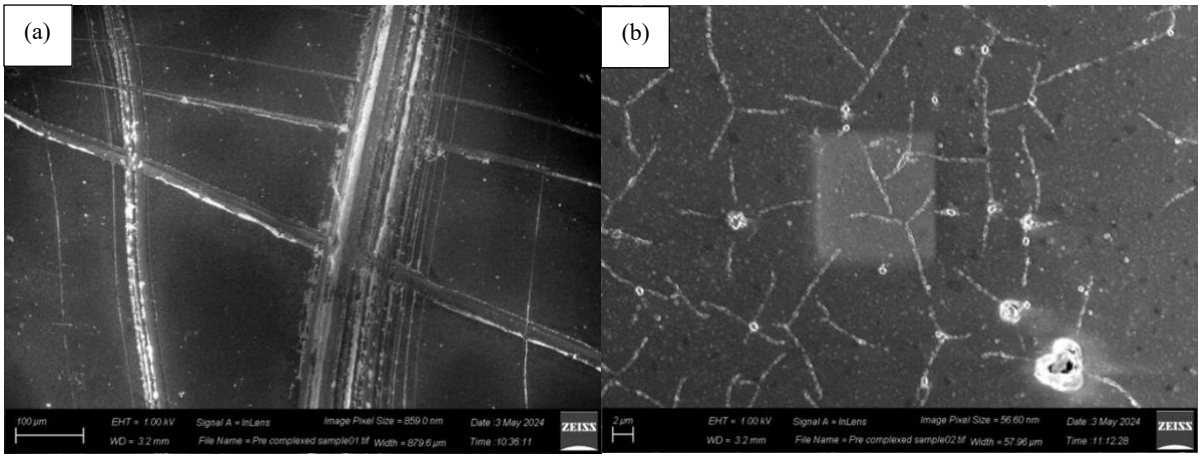

Figure 2. 5(a) and (b): Precomplexed PDMAEMA brushes at different magnifications.

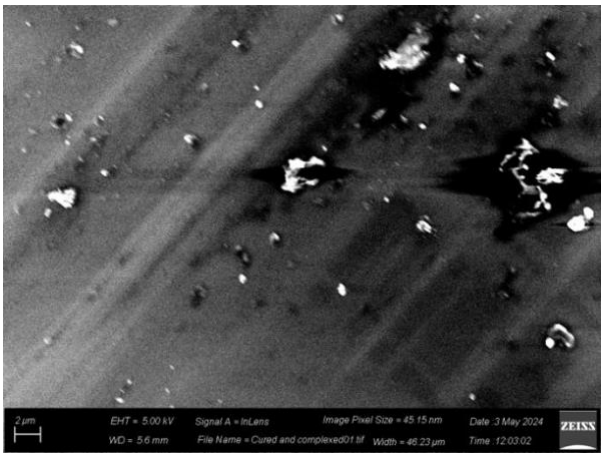

Figure 2. 6: Complexed and cured brush.

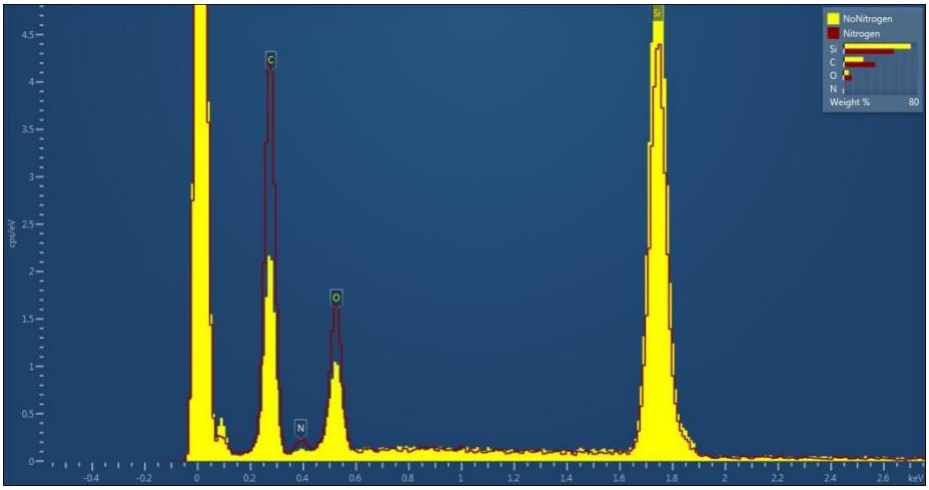

Figure 2. 7: EDX analysis of precomplexed (NoNitrogen) vs. complexed and cured (Nitrogen).

After observing the SEM and EDX results, several things can be noted. Polymer brush growth was observed from the SEM images (see Figure 2.5). However, this polymer brush only contained PDMAEMA. The structure of PDMAEMA clearly suggests that there is no Si element present. So, durazane was used as a complexing agent as it has silicon in its structure. The

tertiary amino groups of PDMAEMA could have acted as hydrogen bond acceptors. While the N-H bonds in Durazane 1800 could have acted as hydrogen bond donors. This could evidence that hydrogen bonding took place, thus forming the complex. A curing step was carried out and the polymer brushes observed in Figure 2.6 evidenced the same. The EDX results proved that the complexed and cured brushes had more nitrogen present, according to the elemental analysis. This further proves that a complexation reaction took place due to the additional nitrogen from the durazane being present.

From the SEM images of the SiC brushes, we could see in Fig 2.8 (a) vs (b) that there was a point where the brush growth stopped on the wafer. Fig 2.9 showed the morphology of the border of the brush crosslinked with allyl methacrylate. From Fig 2.9, we could tell that the brush is thicker at the borders. Fig 2.10 (a), (b), and (c) also showed the different 3D surface morphologies of the crosslinked brush, clearly indicating that the brush was not uniform. Fig 2.11 showed the original vs. annealed regions. Fig 2.12 (a), (b) and (c) showed the morphologies inside each of the three annealed stripes.

It can be noted that the addition of a cross-linker leads to the formation of thicker polymer brushes (Humood et al., 2017). From the SEM images, the cross-linked brush seemed to be thicker and different in morphology. The morphology of the cross-linked brush seems to be non-uniform. This could be due to the cross-linker growth being quicker than the polymer brush growth, thus overtaking the brush growth.

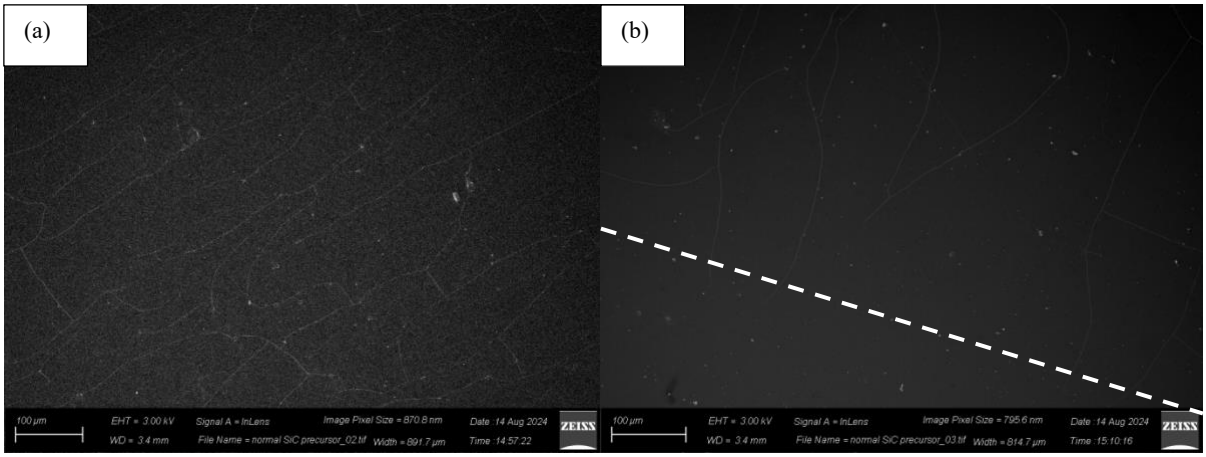

Figure 2. 8(a): Middle section of the wafer and **(b):** Point where brush growth stops.

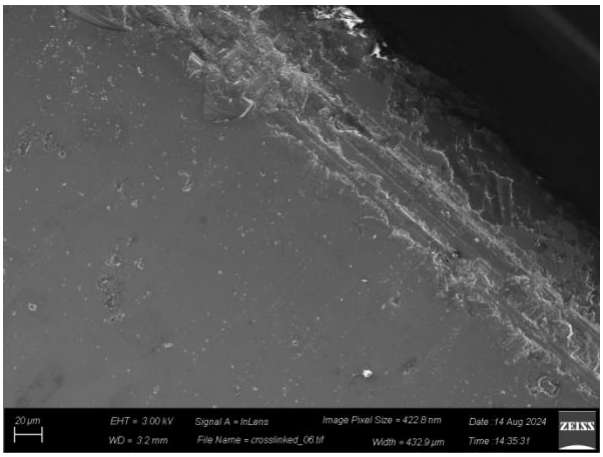

Figure 2. 9: Border of crosslinked polymer brush on wafer.

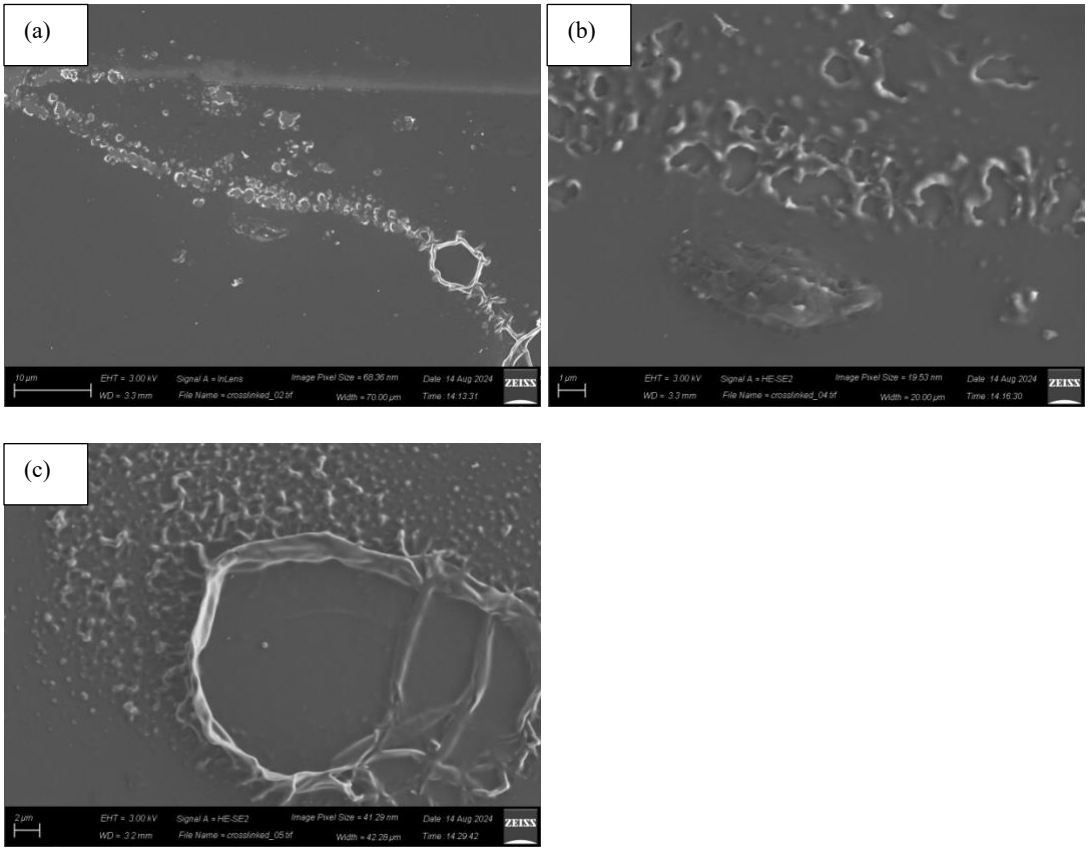

Figure 2. 10 (a), (b) and (c): Different 3D morphologies of the crosslinked brush.

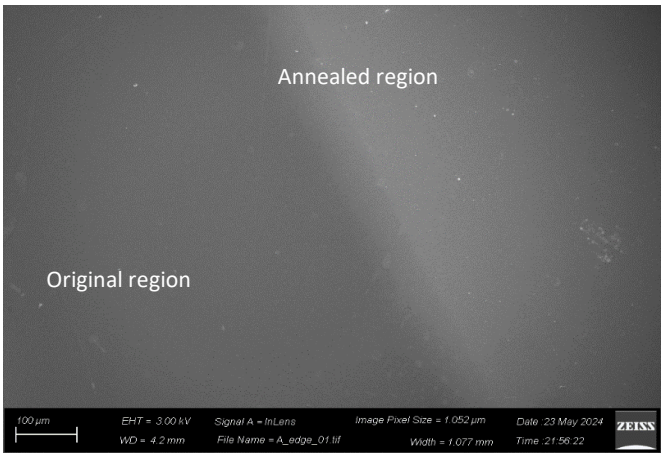

Figure 2. 11: Original vs. Annealed regions.

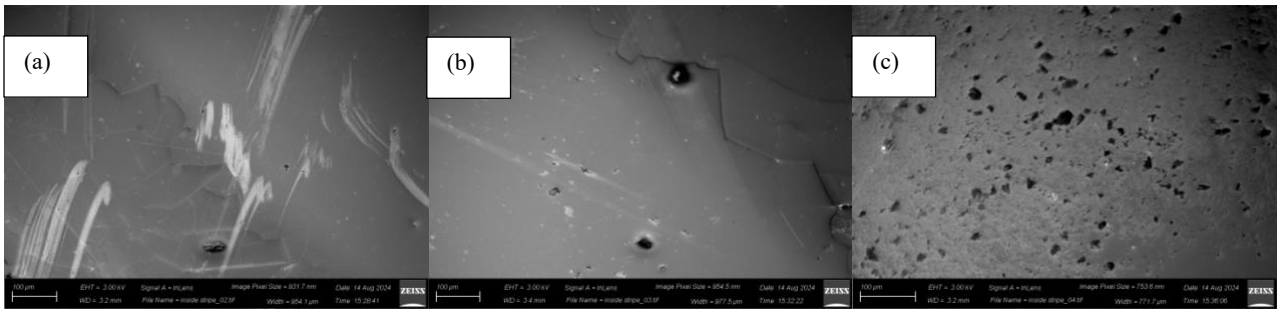

Figure 2. 12 (a), (b) and (c): Inside stripes annealed at varying temperatures from 1200-1300 ^{o}C.

Atomic Force Microscopy: From Fig 2.13, it can be observed that the yellowish region on the brush transitions to the blueish region, indicating a thicker to thinner transition, based on the distance of the copper plate from the treated wafer. The yellowish region is mostly uniform, indicating that there may be a maximum height for brush growth. The brush has grown in a triangular shape, which there is no explanation for. After repeating the same spacer method for polymer brush growth, the next polymer brush also grew in this triangular shape.

Figure 2.14 (b) (amplitude retrace) shows the surface morphology of the blueish region, figure 2.14 (a) shows the height retrace. Figure 2.15 (b) (amplitude retrace) shows the surface morphology of the yellowish region, figure 2.15 (a) shows the height retrace. In terms of morphology, there is a clear difference between the two. Figure 2.15 shows that the yellowish region has a more porous structure. Figure 2.14, on the other hand, seems flatter and less porous. The structure seems like it may be more like a silicon wafer with nothing on top. But the areas with the indents mean that there is probably a very thin brush on top.

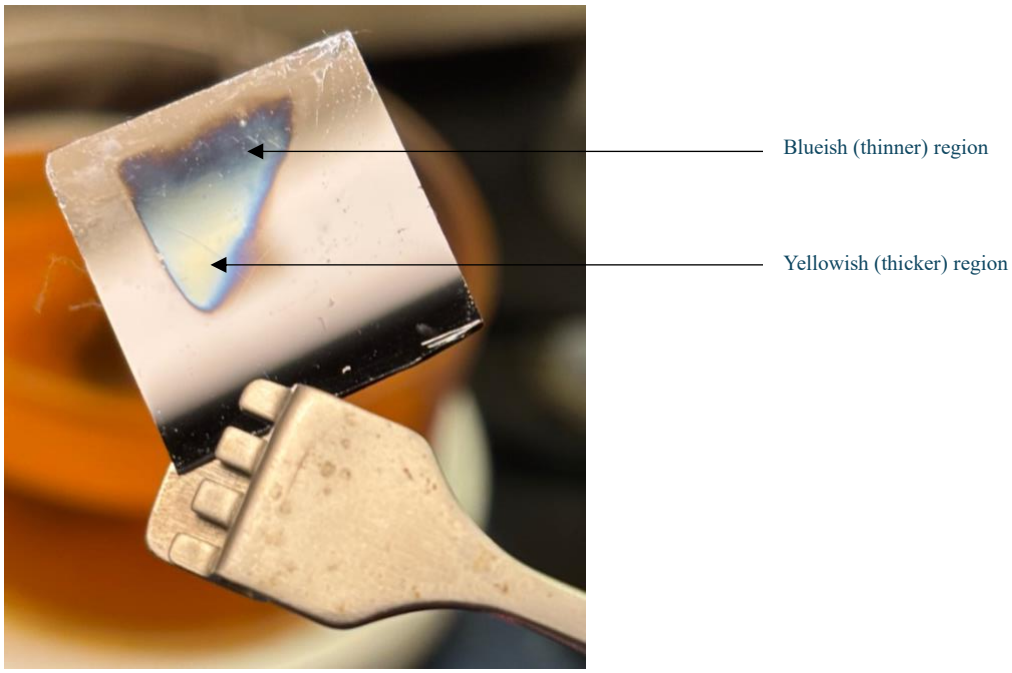

Figure 2. 13: Polymer brush growth using spacer.

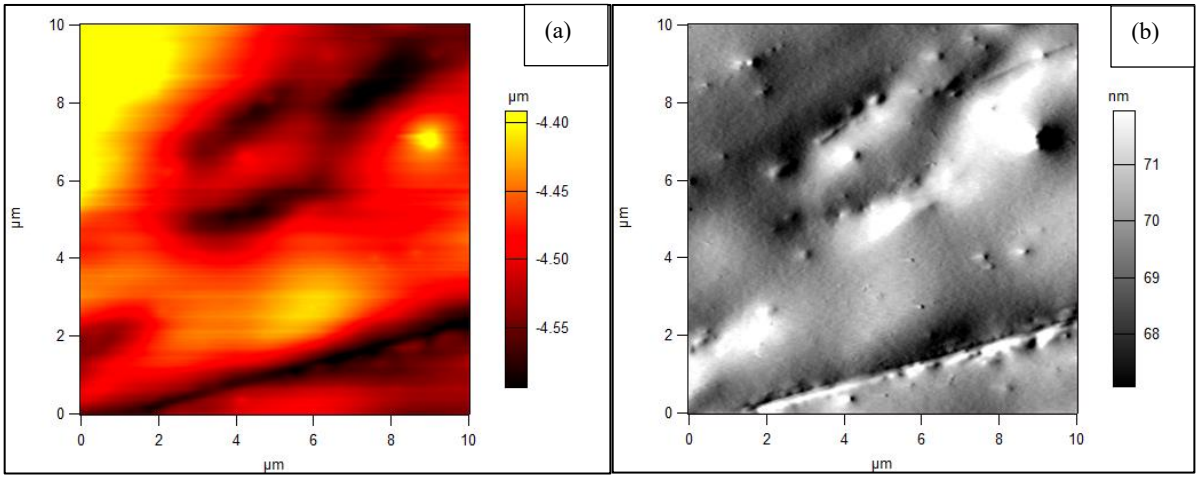

Figure 2. 14(a): Blueish (thinner) region height retrace and **(b):** blueish (thinner) region amplitude retrace (see Figure 2. 13 for blueish region).

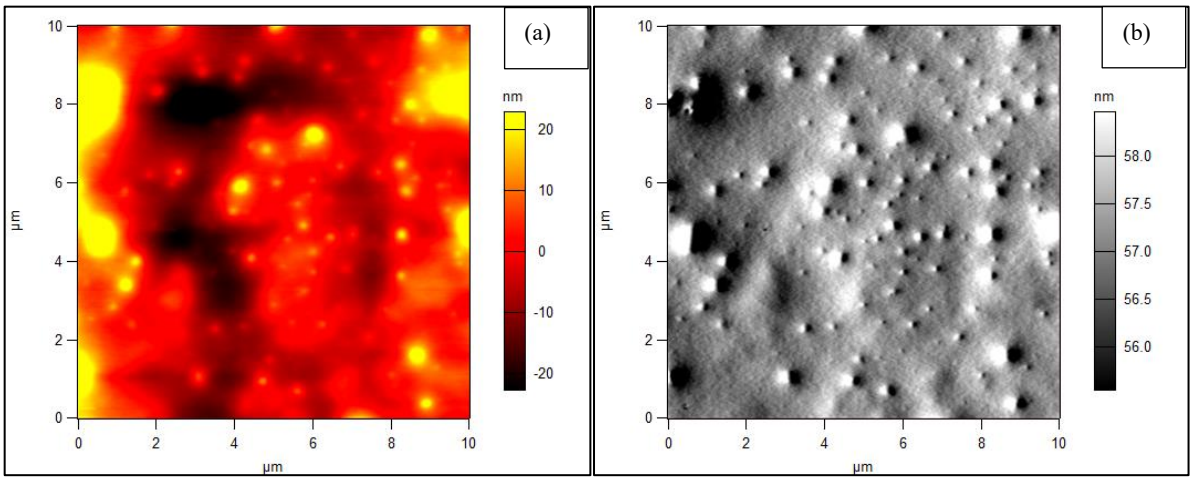

Figure 2. 15 (a): Yellowish (thicker) region height retrace and **(b):** yellowish (thicker) region amplitude retrace (see Figure 2. 13 for yellowish region).

Profilometry: The profilometry result showed that the scratch presented a dip, which could be considered as the lowest point. The heights of the brush reported using this method were in the ranges of 1200-1300 Å. This proves that the brush was mostly uniform in the yellowish region. As the end goal would be to be able to grow a brush that is completely uniform, the profilometry result tells us how thick the uniform brush would be. This could act as a potential template for future brush growth.

X-ray Photoelectron Spectroscopy: Finally, the XPS results of both the brushes were observed. Fig 2.16 showed the various binding energies for the pre-complexed, post-complexed and annealed SiNPBs. Through this data, it can be concluded that laser annealing does have a definitive effect. It shows that the nitrogen peak is missing in the annealed polymer brush. This could occur if for some reason, the annealing causes the polymer brush layer to burn off. Also,

from Fig 2.17, it can be concluded that laser annealing may burn off the polymer brush layer, especially at higher temperatures to expose the Si element as shown by the arrow. The difference between annealed point 1 and annealed point 2 is only the annealing temperature and as mentioned, the higher temperature has given rise to a bigger peak at ~99.4 eV binding energy. (*Carbon | XPS Periodic Table - US*, 2024; *Nanolayers of Poly(N,N'-Dimethylaminoethyl Methacrylate) with a Star Topology and Their Antibacterial Activity*, n.d.; *Nitrogen | XPS Periodic Table - US*, 2024; *Oxygen | XPS Periodic Table - US*, 2024; *Silicon | Periodic Table - US*, 2024; Teper et al., 2020; Yan et al., 2004).

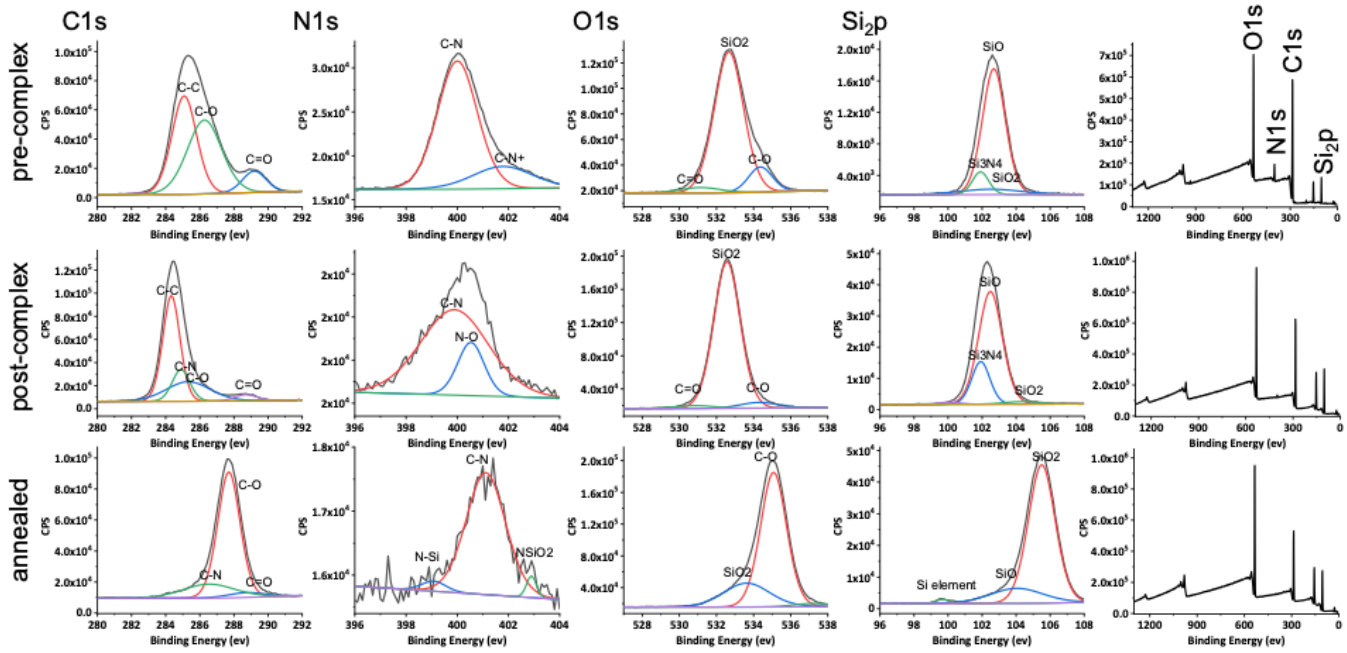

Figure 2. 16: XPS data (carbon, nitrogen, oxygen and silicon) for pre-complexed, post-complexed and annealed SiNPBs.

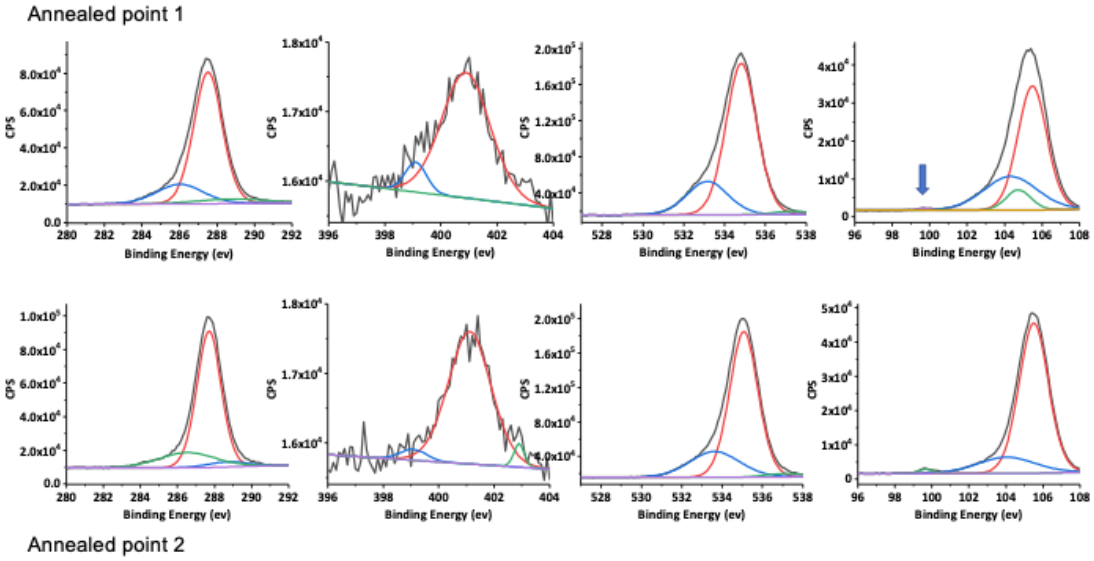

Figure 2. 17: XPS data (carbon, nitrogen, oxygen and silicon) for the two annealed points on the SiNPB.

From Fig 2.18, it was observed that the XPS data for the unannealed vs. annealed points. It was also noted that the presence of Si can be seen in the annealed Si2p XPS spectrum, which means that the laser may be burning off the polymer brush and exposing the silicon wafer but the presence of silicon nitride was also observed (*Carbon | XPS Periodic Table - US*, 2024; *Nitrogen | XPS Periodic Table - US*, 2024; *Oxygen | XPS Periodic Table - US*, 2024; *Silicon | Periodic Table - US*, 2024).

From the data observed for the SiCPB and the SiNPB, it became clear that neither of them was able to handle the high temperature annealing. While both showed that the SiC_xN_y structures were able to be formed, the firing conditions may not have been ideal. To solve this problem, cross-linking the polymer brush would be useful. Cross-linking has proven to be useful as it

improves thickness (Humood et al., 2017) and helps grow high chain density polymer brushes by improving the initiator density (Sweat et al., 2013).

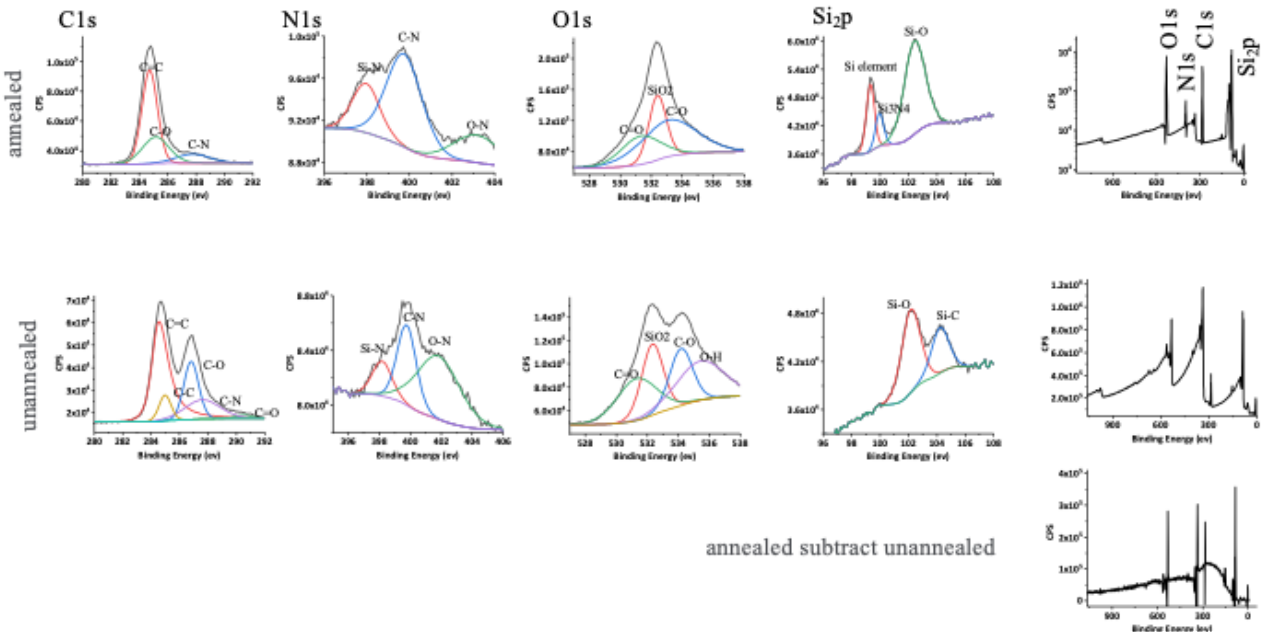

Figure 2. 18: XPS data (carbon, nitrogen, oxygen and silicon) for unannealed vs. annealed points for SiCPBs.

2.4 Conclusion

The effective conversion of surface-grafted preceramic polymer brushes to ceramics using laser annealing on silicon wafers demonstrates the method's potential as a fast and effective approach to ceramic production. PDMAEMA complexed with Durazane and a SiC precursor were used to create two separate types of preceramic brushes—SiNPB and SiCPB—via surface functionalization and polymerization methods. Laser spike annealing in regulated nitrogen and

ammonia atmospheres enabled the transformation of these polymer layers into ceramic structures, resulting in noticeable changes in color, chemical content, and surface properties.

SEM, AFM, and XPS characterization techniques revealed the effective incorporation of nitrogen in the PDMAEMA-derived brushes and the SiC-derived brushes' ceramic-like properties. The spacer methodology provided a novel method for evaluating brush thickness gradients and brush uniformity, demonstrating that closeness to the initiator surface is critical for brush growth and morphology. Profilometry and AFM confirmed the brush height and surface topography, which agreed well with optical and spectroscopic measurements.

Furthermore, XPS data provided valuable insights into the effect of annealing temperature on ceramic conversion. Higher temperatures enhanced the intensity of the silicon signal, indicating that the organic layer may have decomposed, and the silicon substrate was exposed. Nonetheless, the retention of nitrogen and carbon in relevant locations lends support to the concept that laser processing can produce SiC_xN_y structures under specific atmospheric conditions.

This chapter provides a solid framework for applying this technology to nanoscale and non-planar substrates, such as nanoparticles, where similar control over polymer brush development and ceramic conversion is sought. Overall, this study demonstrates the flexibility and efficacy of laser-based annealing procedures for the quick and localized creation of polymer-derived ceramics on designed surfaces.

CHAPTER 3: CONVERSION OF SIC PRECERAMIC POLYMER BRUSHES BY LASER ANNEALING ON SILICA NANOPARTICLES

3.1 Introduction

Silica nanoparticles, similar to silicon wafers, are frequently utilized as substrates for developing polymer brushes due to their silicon oxide surfaces. They have high surface area and pore volume, excellent thermal, mechanical, and chemical stability, cost-effectiveness, the ability to encapsulate both hydrophilic and hydrophobic molecules, and many other useful properties (H. Li et al., 2021).

The Stöber method, which was initially reported by Stöber et al., is a popular process for creating monodisperse silica nanoparticles by using ammonia as a catalyst to hydrolyze and condense tetraethyl orthosilicate (TEOS) in alcoholic media (Stöber et al., 1968). By modifying the reaction conditions and precursor concentrations, this technique allows for control over particle size (dos Santos da Silva & dos Santos, 2023). However, a number of modified Stöber techniques have been developed in order to improve control over morphology, dispersity, and functionalization. The tunability of this method lends itself to being used in many applications, such as making silica nanoparticles that are small enough in size so that they can undergo further polymerization to form core-shell structures.

Because of its versatility, simplicity, and broad monomer compatibility, free radical polymerization (FRP) is a popular method for creating polymer-grafted nanoparticles (PGNs). The technique is frequently used to functionalized nanoparticles, such as silica or metal oxides, allowing for customized interfacial characteristics (Abdelsayed et al., 2006; Leventis et al.,

2007). In general, it can be a useful technique for polymerization of "hairy" nanoparticles, i.e. surface functionalized nanoparticles.

In this study, silica nanoparticles are modified to introduce reactive surface groups and subsequently polymerized with 3-(1,1,1,5,5,5-hexamethyl-3-((trimethylsilyl)oxy)trisiloxan-3-yl)propyl methacrylate using mini-emulsion free radical polymerization. This method employs sodium dodecyl sulfate (SDS) as a surfactant to form micelles in solution, facilitated by a solvent exchange process. The result is a set of size-controlled, well-dispersed, polymer-grafted nanoparticles. This scalable approach enables nanoparticle-to-ceramic transformation, assessed through analysis of core-shell architecture, degree of polymerization, and ceramic yield using techniques such as dynamic light scattering, transmission electron microscopy, and thermogravimetric analysis.

3.2 Experimental section

Synthesis of vinyl functionalized silica nanoparticles: Using the Stober process in two slightly different ways, silica nanoparticles with two different sizes were obtained.

Method A: Ethanol (130 mL), and ammonia hydroxide (30 wt%, 11 mL) were mixed in a round-bottom flask. The flask was pre-heated to 60°C in an oil bath with 400 rpm stirring. After stabilizing for 30 minutes, 5 mL of tetraethyl orthosilicate (TEOS) in 5 ml ethanol was rapidly injected into the mixture. The reaction was subjected to vigorous stirring and allowed to proceed for 24 hours, cooled down and, then 3-(trimethoxysilyl) propyl acrylate (5 mL) was added to the dispersion. The mixture was kept stirring overnight at room temperature and then refluxed for 1 hour. Then particles were centrifuged down at 6000 rpm and redispersed in ethanol and

centrifuged again for 3 times to remove excess reagents. The particles, denoted MPS@SiO2, were then dried in a vacuum oven, and stored in a freezer until used (da Silva & Dos Santos, 2023).

Method B: Following the work done by Huber et al., 4 mL (25%) ammonia, 0.14 mL water were added to 80 mL ethanol and stirred at 45°C (for batch 1) and 60°C (for batch 2). 3 mL TEOS was added after 30 minutes of stirring. After letting it react overnight, 0.6 mL 3-(Trimethoxysilyl) propyl acrylate was added, stirring overnight at 45°C (for batch 1) and 60°C (for batch 2) (Hübner et al., 2018).

Change of dispersion media: A solution of SDS/water was prepared and added dropwise into the nanoparticle solution while sonicating. 40 mg of SDS was dissolved in 80 mL water to make the SDS/water solution. After this, the ethanol from the earlier step was completely removed using the rotary evaporator at 80 mbar pressure and 55 ^{o}C temperature. The resulting solution contained the silica nanoparticles dispersed in SDS/water. This solution was allowed to rest overnight (Hübner et al., 2018).

Polymerization of silica nanoparticles: Emulsion polymerization was used to polymerize the silica nanoparticles. 0.2 mL of the SiC monomer (3-(1,1,1,5,5,5-Hexamethyl-3-((trimethylsilyl)oxy)trisiloxan-3-yl)propyl methacrylate) was added to the 80 mL solution of silica nanoparticles dispersed in SDS/water. This was followed by ultrasonication for 20 minutes using the probe sonicator at 0^{o}C. The solution was then degassed using nitrogen gas after which

6 mg of AIBN was added. The solution was degassed again and allowed to stir for 24 hours at 70^{o}C.

Extraction of silica nanoparticles with brushes: The nanoparticles were centrifuged at 4400 rpm for 10 minutes and then washed thrice using ethanol to remove any excess reactants or impurities. These were then dried in the vacuum oven overnight at 30^{o}C.

Material characterization: Dynamic light scattering and **Transmission Electron Microscopy** were used to determine the size of the nanoparticles and the core-shell structures or aggregation respectively. The DLS was done using the Zetasizer (Malvern Nano ZS), using the size mode, setting the material to silica and the solvent to 70% ethanol, 30% water for the pre solvent exchanged nanoparticles and water for the ones post.

The TEM was done using the Thermo Fisher Titan 300 S/TEM (Perseus) at 300 kV. It was done for varying magnifications, from 100 nm to 2 μm, depending on the type of nanoparticles.

Yield was calculated by checking how much TEOS was converted to silica nanoparticles.

To assess the weight % brush content of the nanoparticles, a **thermogravimetric analysis** was carried out. The instrument used was the TA Instruments 5500 Thermogravimetric Analyzer (TGA). The heating rate was 10^{o}C/min and the heating was done from 0 to 600^{o}C in air.

3.3 Results and Discussion

Dynamic Light Scattering: The DLS results have been tabulated for method A vs. B and the brushes in table 3.1. This data shows that while all the methods could grow silica nanoparticles in the nano ranges, Method A and Method B (batch 2) had the right particle size for the polymer brushes grown on silica nanoparticles, i.e. nano size post polymer brush growth.

Method	Sample	Diameter (nm)	PDI
Method A	Silica nanoparticles	115	0.029
Method A	Silica nanoparticles+ 3-(trimethoxysilyl) propyl methacrylate emulsion	139	0.029
Method A	Polymer brush grown on silica nanoparticles	258.7	0.201
Method B (batch 1)	Silica nanoparticles	104.6	0.007
Method B (batch 1)	Silica nanoparticles+ 3-(trimethoxysilyl) propyl methacrylate emulsion	111	0.025
Method B (batch 1)	Polymer brush grown on silica nanoparticles	>1k	0.505

Method B (batch 2)	Silica nanoparticles	62	0.032
Method B (batch 2)	Silica nanoparticles+ 3-(trimethoxysilyl) propyl methacrylate emulsion	64	0.030
Method B (batch 2)	Polymer brush grown on silica nanoparticles	228	0.372

Table 3.1: Particle size results.

Transmission Electron Microscopy: The TEM data collected using method A can be observed in figures 3.1 and 3.2. In Fig 3.1(a) and (b), it shows the original nanoparticles and their aggregation. Fig 3.2 (a) and (b) show the core-shell structure of the polymerized nanoparticles. These structures were the desired core-shell type and were the appropriate size, still being measured at the nano scale.

The TEM data collected using method B (batch 1), can be observed in figures 3.3, 3.4 and 3.5. Fig 3.1(a) and (b) shows the original nanoparticles. Fig 3.4 shows the aggregated nanoparticles post polymerization. Fig 3.5 (a) and (b) show the core-shell structure of the polymerized nanoparticles. The shaded portion surrounding the nanoparticles is the shell and the nanoparticles are the core.

The TEM data collected using method B (batch 2), can be observed in figures 3.6 and 3.7. Figure 3.6 shows some aggregation in the original nanoparticles. Figure 3.7 (a) shows that while polymer growth may have occurred, it did not occur only on the nanoparticle surface but all

throughout the solution in which the nanoparticles were dispersed. This can be observed by zooming into the aggregated structure, as observed in Figure 3.7 (b).

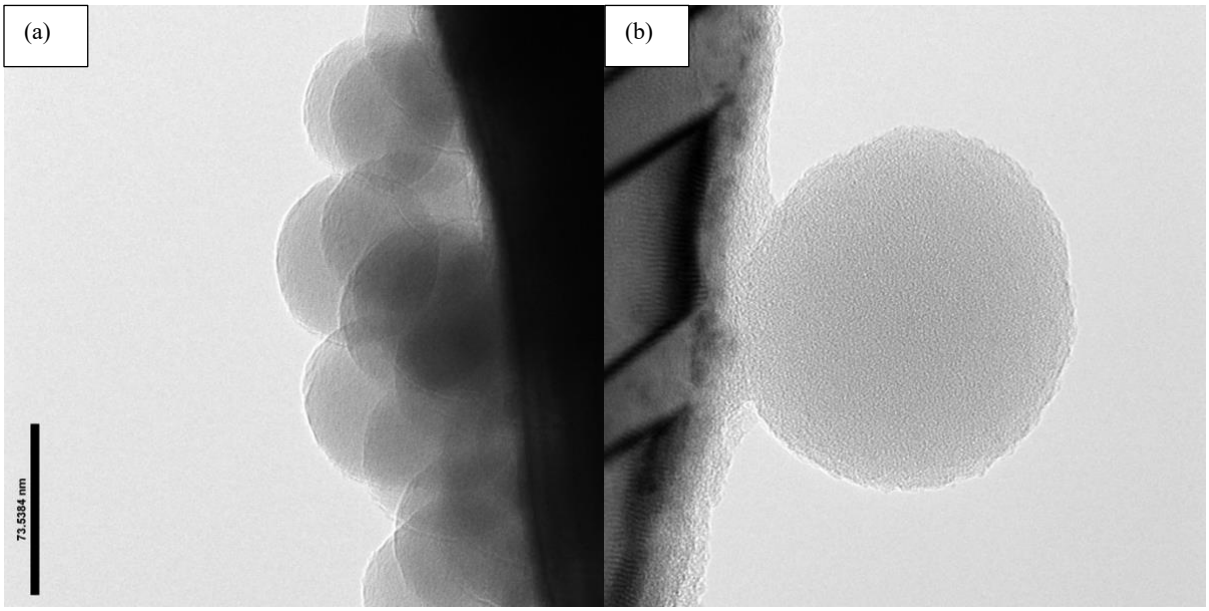

Figure 3. 1(a) and (b): Original nanoparticle images, method A.

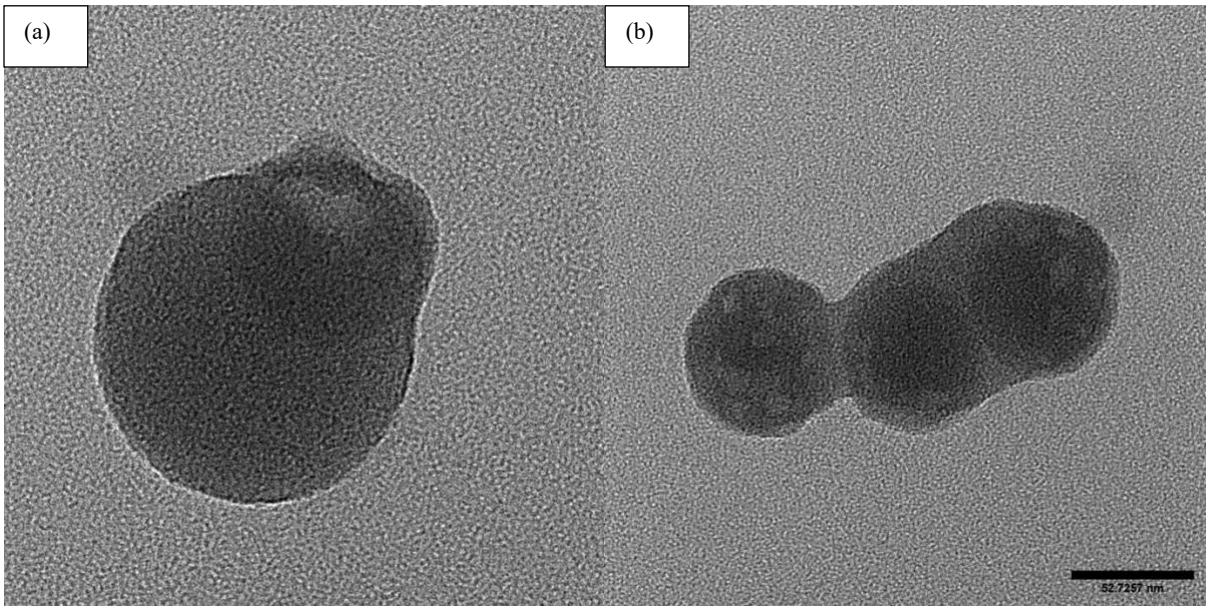

Figure 3. 2 (a) and (b): Core-shell structure of polymerized nanoparticles, method A.

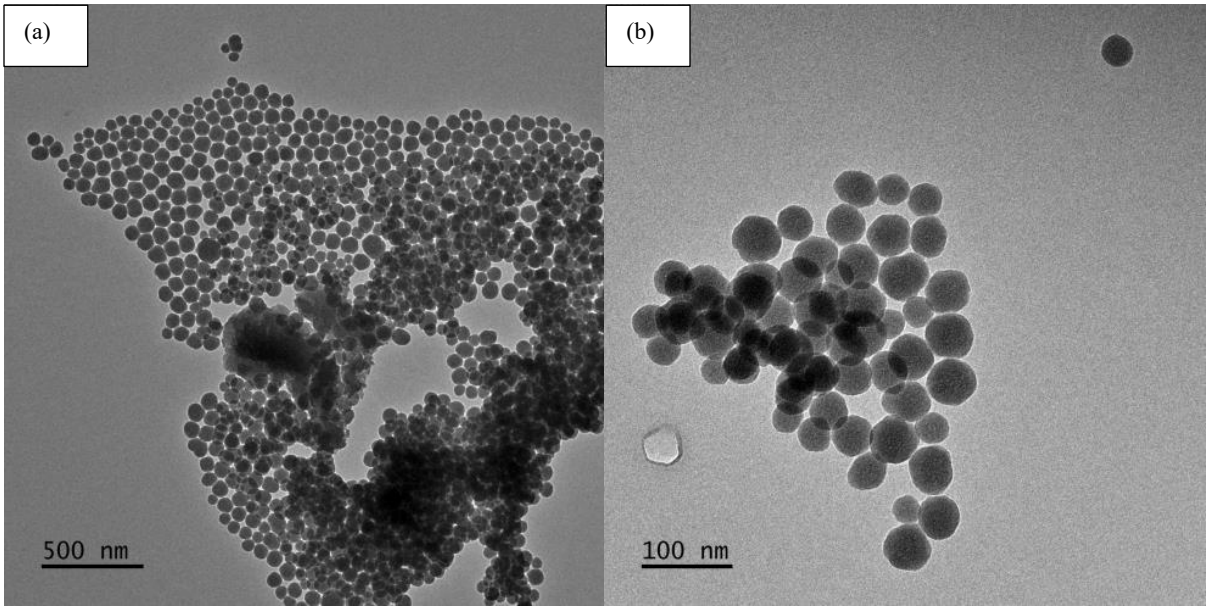

Figure 3. 3(a) and (b): Original nanoparticle images, method B (batch 1).

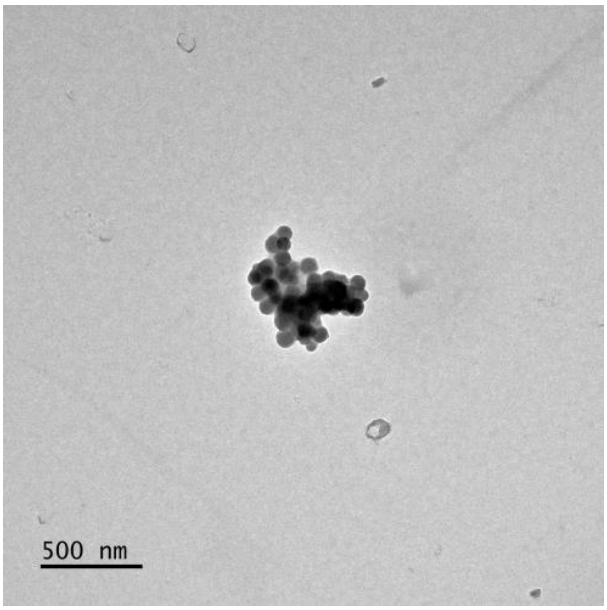

Figure 3. 4: Aggregated nanoparticles post polymerization without brush, method B (batch 1).

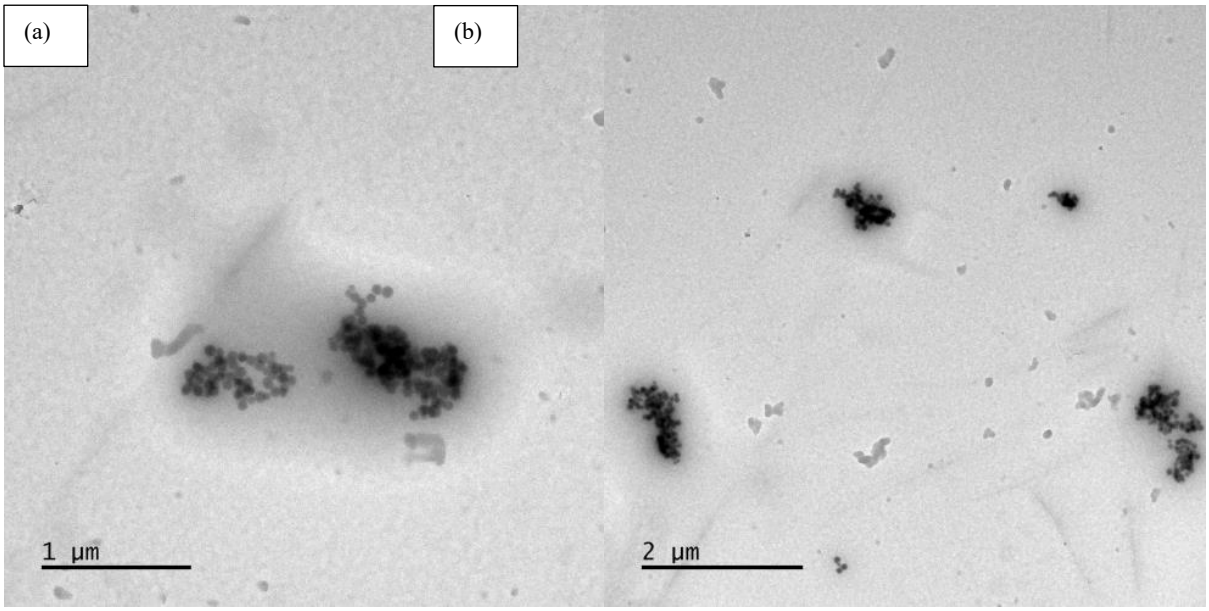

Figure 3. 5 (a) and (b): Core-shell structure of polymerized nanoparticles, method B (batch 1).

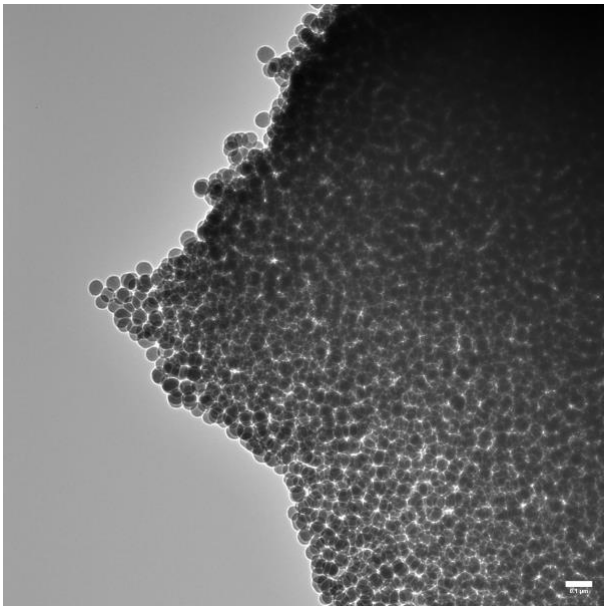

Figure 3. 6: Original nanoparticle images, method B (batch 2).

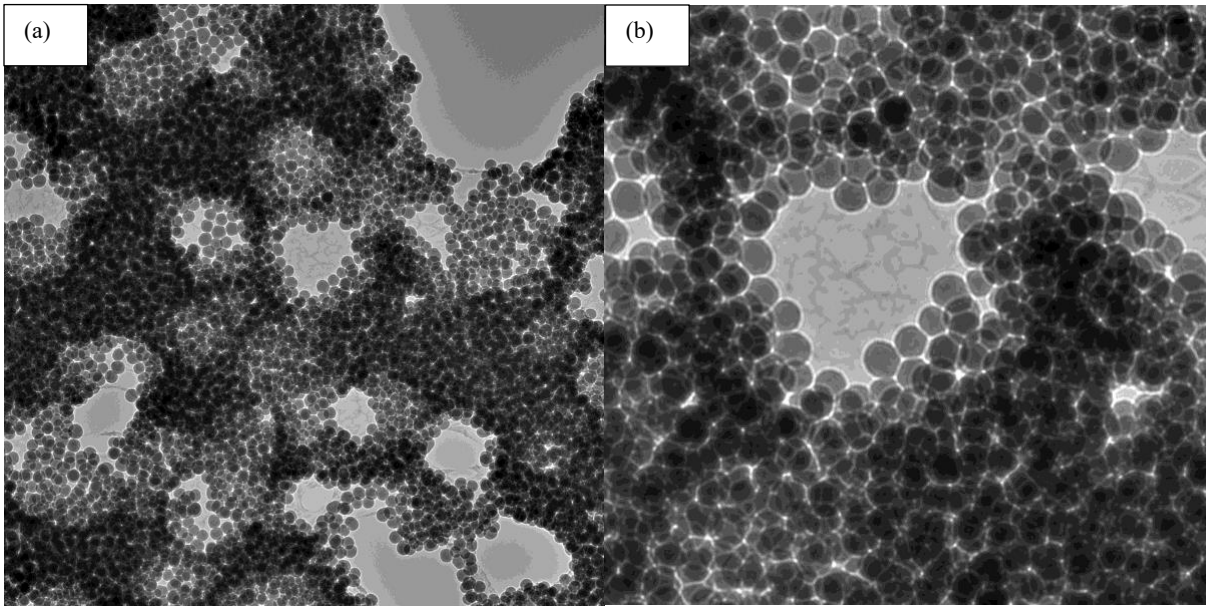

Figure 3. 7(a): Polymerized nanoparticles, method B (batch 2) and **(b):** Zoomed in image of the aggregated structure caused by polymerization.

Yield of nanoparticles from method A vs. B: From method A, yield was ~99% but from method B, yield was ~10%. The reaction with the higher yield is thus more desirable.

Thermogravimetric Analysis: Only method A and method B (batch 1) was used for the TGA. From method A, we can observe that the organic portion in the polymer brush grown on silica nanoparticles is 54.84%, as shown in Fig 3.8. From method B (batch 1), we can observe that the organic portion in the polymer brush grown on silica nanoparticles is 64.99%. This means that method B (batch 1) was able to form a thicker brush, which matches the DLS particle size results (as particle size was >1k nm). This, in turn, means that a higher percentage of brush growth does not necessarily mean that the growth in controlled or uniform, as observed in the TEM images too. From method B (batch 1), the polymer brush part was 13.9%, as shown in Fig 3.9 (a) and (b).

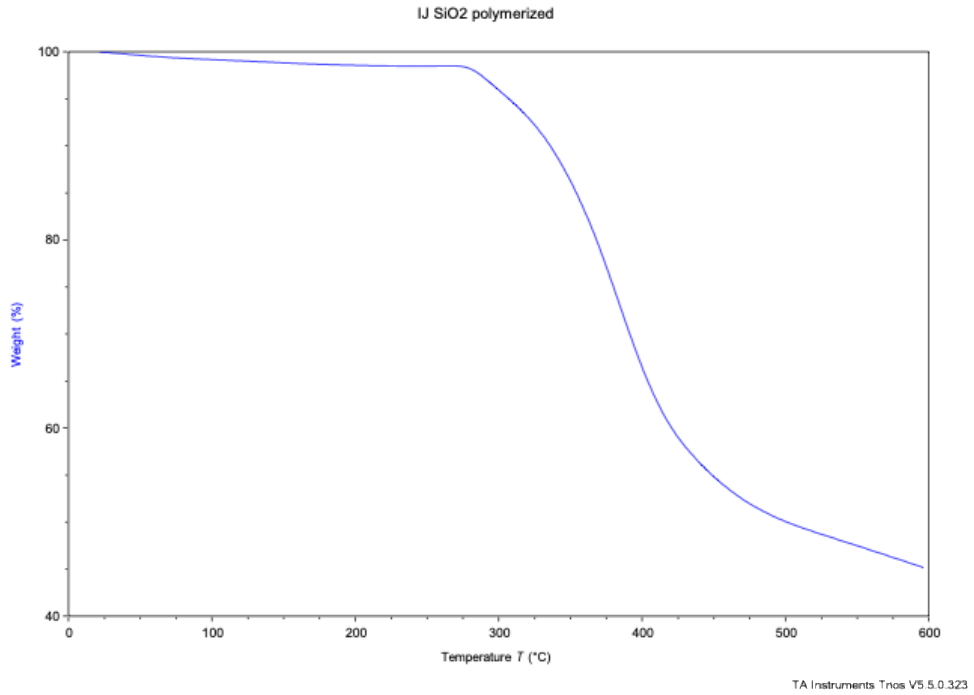

Figure 3. 8: Polymerized silica nanoparticles.

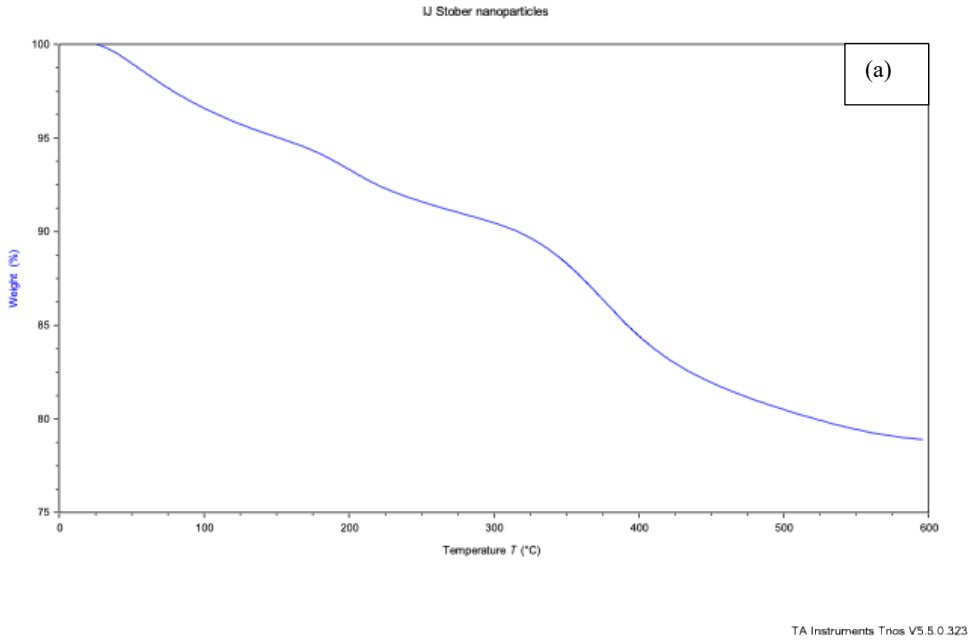

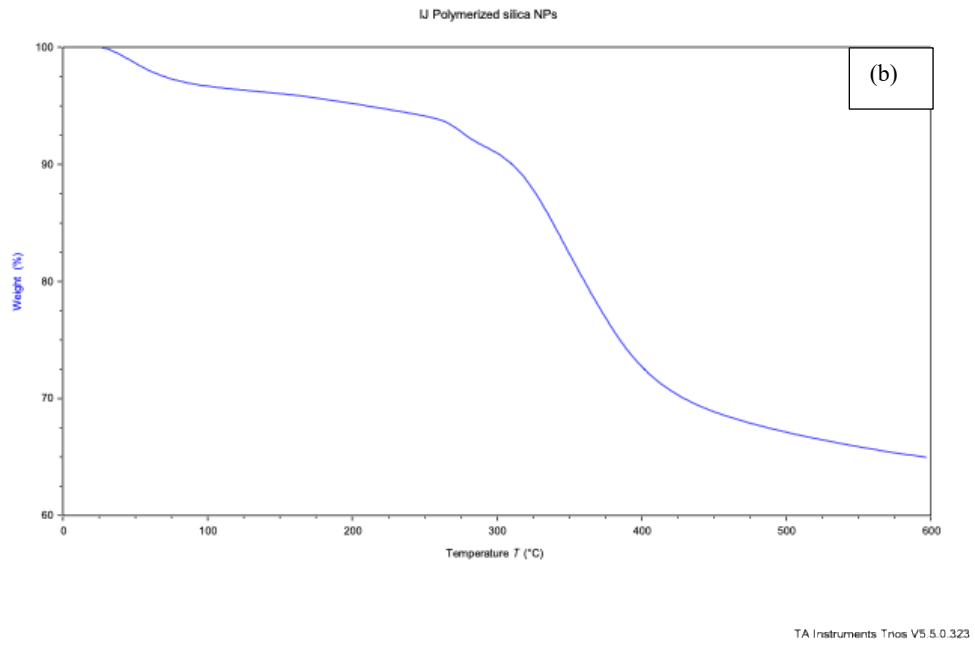

Figure 3. 9 (a): Original silica nanoparticles and **(b):** Polymerized nanoparticles.

3.4 Conclusion

This chapter demonstrated the design, synthesis, and polymerization of silica nanoparticles into polymer-grafted nanostructures, which were then successfully transformed into ceramic materials using a mini-emulsion free radical polymerization approach. Building on Chapter 2's planar wafer-based methodology, this study expanded the conversion of preceramic polymers to ceramic structures on three-dimensional nanoparticle substrates—an important step toward practical, scalable applications of polymer-derived ceramics in nanotechnology.

Monodisperse silica nanoparticles of various sizes were produced using two variants of the Stöber technique before being functionalized with vinyl groups to allow surface polymerization. The incorporation of the SiC monomer with sodium dodecyl sulfate as a surfactant resulted in core-shell structures, which were validated by dynamic light scattering and high-resolution TEM

investigation. Polymer shell development considerably enhanced particle size and caused morphological changes consistent with effective grafting.

Method A was the most effective procedure for scalable manufacturing due to its controlled particle dispersion, high yield (~99%), and appropriate polymer loading (~55% organic content by TGA). It also gave nanoparticles with core-shell structures that were of nano size as well, which was extremely desirable. In contrast, Method B, while valuable in displaying variability, had reduced polymer content and increased aggregation, particularly in batch 2, where uncontrolled polymerization across the matrix suggested difficulties with surface-specific grafting.

In conclusion, this work validates a robust, scalable strategy for synthesizing polymer-grafted ceramic nanoparticles with tunable core–shell architecture. It paves the way for future research into integrating different functional nanoparticle cores, such as optoelectronic or catalytic materials, which will widen the utility of this method for a wide range of high-performance applications.

CHAPTER 4: FUTURE WORK

This research explores the rapid transformation of preceramic polymer brushes and brush-functionalized silica nanoparticles into ceramic materials using laser annealing. This work proposes an effective, scalable method for producing nanostructured ceramic materials, with potential applications in advanced coatings, nanocomposites, and high-performance materials engineering.

As a first step in future work, it would be valuable to optimize the cross-linking of the polymer brushes formed on silicon wafers. Preliminary attempts at cross-linking were made; however, the results were suboptimal. It appears that the cross-linker interfered with the polymerization process, preventing the proper formation of the brush layer. Exploring alternative cross-linkers may improve the stability and integrity of the brushes, potentially leading to more robust structures that withstand laser annealing without degradation of the brush layer.

Another potential direction for future work involves the annealing of core-shell nanoparticles to convert the preceramic polymer shell into a stable ceramic layer. Several thermosetting and pyrolysis approaches can be employed for this purpose. For instance, Martin et al. demonstrated a simple method involving vacuum drying of the nanoparticles on a glass slide to initiate curing (Martin et al., 2022). A more robust technique involves annealing in a tube furnace under an inert atmosphere (e.g., nitrogen or argon), as demonstrated by Yu et al., which enables controlled thermal conversion of the shell (Z. Yu et al., 2022). Additionally, laser annealing, widely used for nanostructured films and particles, offers localized and rapid heating; for example, Bigot et al. (2012) employed a Titanium-Sapphire laser to effectively anneal CoPt nanoparticles (Bigot et al.,

2012). These methods illustrate a range of thermal treatment strategies, each offering distinct advantages in terms of shell morphology, ceramic yield, and structural preservation.

Nanoparticles with different properties may be used in the future as the core, instead of silica. For example, ZnSe or ZnS nanoparticles possess useful optical properties. In its bulk state, ZnSe has a direct bandgap of around 2.7 eV, which allows for significant absorption in the visible and ultraviolet (UV) spectrums. In their nanoparticle form, ZnSe displays quantum confinement effects enable precise tweaking of optical characteristics by causing a blue shift in both absorption and emission spectra (Chi et al., 2021). Due to these properties, ZnSe can be used as UV photodetectors and have photocatalytic application. This may provide these unique core-shell nanoparticles with properties tunable for both the core and the shell.

REFERENCES

Abdelsayed, V., Alsharaeh, E., & El-Shall, M. S. (2006). Catalyzed Radical Polymerization of Styrene Vapor on Nanoparticle Surfaces and the Incorporation of Metal and Metal Oxide Nanoparticles within Polystyrene Polymers. The Journal of Physical Chemistry B, 110(39), 19100–19103. https://doi.org/10.1021/jp064720p

Ackley, B. J., Martin, K. L., Key, T. S., Clarkson, C. M., Bowen, J. J., Posey, N. D., Ponder Jr., J. F., Apostolov, Z. D., Cinibulk, M. K., Pruyn, T. L., & Dickerson, M. B. (2023). Advances in the Synthesis of Preceramic Polymers for the Formation of Silicon-Based and Ultrahigh-Temperature Non-Oxide Ceramics. Chemical Reviews, 123(8), 4188–4236. https://doi.org/10.1021/acs.chemrev.2c00381

Ainger, F. W., & Herbert, J. M. (1960). Special ceramics. By P. Popper, Academic Press, New York, 168.

Aktas Eken, G., & Ober, C. K. (2022). Strong Polyelectrolyte Brushes via Alternating Copolymers of Styrene and Maleimides: Synthesis, Properties, and Stability. Macromolecules, 55(13), 5291–5300. https://doi.org/10.1021/acs.macromol.2c00647

A. Nayl, A., I. Abd-Elhamid, A., A. Aly, A., & Bräse, S. (2022). Recent progress in the applications of silica-based nanoparticles. RSC Advances, 12(22), 13706–13726. https://doi.org/10.1039/D2RA01587K

Bell, A. E. (1979). Review and analysis of laser annealing. Rca Review, 40(3), 295.

Bigot, J.-Y., Kesserwan, H., Halté, V., Ersen, O., Moldovan, M. S., Kim, T. H., Jang, J., & Cheon, J. (2012). Magnetic Properties of Annealed Core–Shell CoPt Nanoparticles. Nano Letters, 12(3), 1189–1197. https://doi.org/10.1021/nl300306a

Blum, Y. D., Schwartz, K. B., & Laine, R. M. (1989). Preceramic polymer pyrolysis: Part 1 Pyrolytic properties of polysilazanes. Journal of Materials Science, 24, 1707–1718.

Bombalski, L., Dong, H., Listak, J., Matyjaszewsk, K., & Bockstaller, M. R. (2007). Null-Scattering Hybrid Particles Using Controlled Radical Polymerization. Advanced Materials, 19(24), 4486–4490. https://doi.org/10.1002/adma.200700928

Bowen, J. J., Rueschhoff, L. M., Martin, K. L., Street, D. P., Patel, T. A., Parvulescu, M. J. S., Bedford, N. M., Koerner, H., Seifert, S., & Dickerson, M. B. (2020). Tailorable Micelle Morphology in Self-Assembling Block Copolymer Gels for Templating Nanoporous Ceramics. Macromolecules, 53(17), 7528–7536. https://doi.org/10.1021/acs.macromol.0c01137

Brittain, W. J., & Minko, S. (2007). A structural definition of polymer brushes. Journal of Polymer Science Part A: Polymer Chemistry, 45(16), 3505–3512. https://doi.org/10.1002/pola.22180

Carbon | XPS Periodic Table—US. (2024). https://www.thermofisher.com/us/en/home/materials-science/learning-center/periodic-table/non-metal/carbon.html

Chi, T. T. K., Hien, B. T. T., Nam, M. H., & Hai, P. N. (2021). Structural and Optical Properties of ZnSe Nanoparticles. Journal of Nanoscience and Nanotechnology, 21(4), 2582–2587. https://doi.org/10.1166/jnn.2021.19114

da Silva, A. dos S., & Dos Santos, J. H. Z. (2023). Stöber method and its nuances over the years. Advances in Colloid and Interface Science, 314, 102888.

dos Santos da Silva, A., & dos Santos, J. H. Z. (2023). Stöber method and its nuances over the years. Advances in Colloid and Interface Science, 314, 102888. https://doi.org/10.1016/j.cis.2023.102888

Feigenoff, Charlie. (2018, November 1). Generating Current as Well as Thrust from Jet Engines. University of Virginia School of Engineering and Applied Science. https://engineering.virginia.edu/news-events/news/generating-current-well-thrust-jet-engines

Feng, C., & Huang, X. (2018). Polymer Brushes: Efficient Synthesis and Applications. Accounts of Chemical Research, 51(9), 2314–2323. https://doi.org/10.1021/acs.accounts.8b00307

Fritz, G., & Raabe, B. (1956). Bildung siliciumorganischer Verbindungen. V. Die Thermische Zersetzung von Si(CH3)4 und Si(C2H5)4. Zeitschrift für anorganische und allgemeine Chemie, 286(3–4), 149–167. https://doi.org/10.1002/zaac.19562860307

Hübner, C., Fettkenhauer, C., Voges, K., & Lupascu, D. C. (2018). Agglomeration-Free Preparation of Modified Silica Nanoparticles for Emulsion Polymerization—A Well Scalable Process. Langmuir, 34(1), 376–383. https://doi.org/10.1021/acs.langmuir.7b03753

Humood, M., Qin, S., Song, Y., Polychronopoulou, K., Zhang, Y., Grunlan, J. C., & Polycarpou, A. A. (2017). Influence of Graphene Reduction and Polymer Cross-Linking on Improving the Interfacial Properties of Multilayer Thin Films. ACS Applied Materials & Interfaces, 9(1), 1107–1118. https://doi.org/10.1021/acsami.6b13209

Jacobs, A. G., Jung, B., Jiang, J., Ober, C. K., & Thompson, M. O. (2015). Control of polystyrene-block-poly (methyl methacrylate) directed self-assembly by laser-induced millisecond thermal annealing. Journal of Micro/Nanolithography, MEMS, and MOEMS, 14(3), 031205–031205.

Jakab, P. L. (1997). Visions of a Flying Machine: The Wright Brothers and the Process of Invention. Smithsonian Institution.

Jakša, G., Štefane, B., & Kovač, J. (2013). XPS and AFM characterization of aminosilanes with different numbers of bonding sites on a silicon wafer. Surface and Interface Analysis, 45(11–12), 1709–1713. https://doi.org/10.1002/sia.5311

Jiang, J., Jung, B., Thompson, M. O., & Ober, C. K. (2013). Line edge roughness of high deprotection activation energy photoresist by using sub-millisecond post exposure bake. Advances in Resist Materials and Processing Technology XXX, 8682, 443–449. https://www.spiedigitallibrary.org/conference-proceedings-of-spie/8682/86821N/Line-edge-roughness-of-high-deprotection-activation-energy-photoresist-by/10.1117/12.2011667.short

Jung, B., Chandhok, M., Younkin, T. R., Ober, C. K., & Thompson, M. O. (2011). Time dependent behavior of chemically amplified resist characterized under sub-millisecond post exposure bake. Journal of Photopolymer Science and Technology, 24(5), 487–490.

Jung, B., Satish, P., Bunck, D. N., Dichtel, W. R., Ober, C. K., & Thompson, M. O. (2014). Laser-Induced Sub-millisecond Heating Reveals Distinct Tertiary Ester Cleavage Reaction Pathways in a Photolithographic Resist Polymer. ACS Nano, 8(6), 5746–5756. https://doi.org/10.1021/nn500549w

Jung, B., Sha, J., Paredes, F., Chandhok, M., Younkin, T. R., Wiesner, U., Ober, C. K., & Thompson, M. O. (2012). Kinetic Rates of Thermal Transformations and Diffusion in Polymer Systems Measured during Sub-millisecond Laser-Induced Heating. ACS Nano, 6(7), 5830–5836. https://doi.org/10.1021/nn300008a

Jung, B., Sha, J., Paredes, F., Ober, C. K., Thompson, M. O., Chandhok, M., & Younkin, T. R. (2010). Sub-millisecond post exposure bake of chemically amplified resists by CO2 laser heat treatment. Advances in Resist Materials and Processing Technology XXVII, 7639,

194–202. https://www.spiedigitallibrary.org/conference-proceedings-of-spie/7639/76390L/Sub-millisecond-post-exposure-bake-of-chemically-amplified-resists-by/10.1117/12.848418.short

Kane, K. A., Pint, B. A., Mitchell, D., & Haynes, J. A. (2021). Oxidation of ultrahigh temperature ceramics: Kinetics, mechanisms, and applications. Journal of the European Ceramic Society, 41(13), 6130–6150. https://doi.org/10.1016/j.jeurceramsoc.2021.05.055

Kankala, R. K., Han, Y.-H., Na, J., Lee, C.-H., Sun, Z., Wang, S.-B., Kimura, T., Ok, Y. S., Yamauchi, Y., Chen, A.-Z., & Wu, K. C.-W. (2020). Nanoarchitectured Structure and Surface Biofunctionality of Mesoporous Silica Nanoparticles. Advanced Materials, 32(23), 1907035. https://doi.org/10.1002/adma.201907035

Lécuyer, E., Yoshida, H., Parthasarathy, N., Alm, C., Babak, T., Cerovina, T., Hughes, T. R., Tomancak, P., & Krause, H. M. (2007). Global analysis of mRNA localization reveals a prominent role in organizing cellular architecture and function. Cell, 131(1), 174–187.

Leventis, N., Sotiriou-Leventis, C., & Mulik, S. (2007). Crosslinking 3D assemblies of silica nanoparticles (aerogels) by surface-initiated free radical polymerization of styrene and methylmethacrylate. https://scholarsmine.mst.edu/chem_facwork/2362/

Li, A., Benetti, E. M., Tranchida, D., Clasohm, J. N., Schönherr, H., & Spencer, N. D. (2011). Surface-Grafted, Covalently Cross-Linked Hydrogel Brushes with Tunable Interfacial and Bulk Properties. Macromolecules, 44(13), 5344–5351. https://doi.org/10.1021/ma2006443

Li, H., Chen, X., Shen, D., Wu, F., Pleixats, R., & Pan, J. (2021). Functionalized silica nanoparticles: Classification, synthetic approaches and recent advances in adsorption applications. Nanoscale, 13(38), 15998–16016. https://doi.org/10.1039/D1NR04048K

Li, L., Wang, W., Tang, J., Wang, Y., Liu, J., Huang, L., Wang, Y., Guo, F., Wang, J., Shen, W., & Belfiore, L. A. (2019). Classification, Synthesis, and Application of Luminescent Silica Nanoparticles: A Review. Nanoscale Research Letters, 14(1), 190. https://doi.org/10.1186/s11671-019-3006-y

Lovell, P. A., & Schork, F. J. (2020). Fundamentals of Emulsion Polymerization. Biomacromolecules, 21(11), 4396–4441. https://doi.org/10.1021/acs.biomac.0c00769

Martin, K. L., Street, D. P., Thompson, C. M., Parvulescu, M. J. S., & Dickerson, M. B. (2022). Impact of the Backbone Structure on the Rheological and Thermal Properties of Preceramic Polymer-Grafted Nanoparticles and Derived Ceramics. ACS Applied Nano Materials, 5(1), 446–454. https://doi.org/10.1021/acsanm.1c03278

Matyjaszewski, K., & Xia, J. (2001). Atom Transfer Radical Polymerization. Chemical Reviews, 101(9), 2921–2990. https://doi.org/10.1021/cr940534g

Mera, G., & Ionescu, E. (2019). Polymer-Derived Ceramics. In R. A. Scott (Ed.), Encyclopedia of Inorganic and Bioinorganic Chemistry (2nd ed., pp. 1–26). Wiley. https://doi.org/10.1002/9781119951438.eibc2705

Nanolayers of Poly(N,N′-Dimethylaminoethyl Methacrylate) with a Star Topology and Their Antibacterial Activity. (n.d.). Retrieved February 26, 2025, from https://www.mdpi.com/2073-4360/12/1/230

Narayan, J., Young, R. T., & White, C. W. (1978). A comparative study of laser and thermal annealing of boron-implanted silicon. Journal of Applied Physics, 49(7), 3912–3917. https://doi.org/10.1063/1.325398

Nitrogen | XPS Periodic Table—US. (2024). https://www.thermofisher.com/us/en/home/materials-science/learning-center/periodic-table/non-metal/nitrogen.html

Oxygen | XPS Periodic Table—US. (2024). https://www.thermofisher.com/us/en/home/materials-science/learning-center/periodic-table/non-metal/oxygen.html

Packirisamy, S., Sreejith, K. J., Devapal, D., & Swaminathan, B. (2020). Polymer-Derived Ceramics and Their Space Applications. In Y. Mahajan & J. Roy (Eds.), Handbook of Advanced Ceramics and Composites (pp. 1–107). Springer International Publishing. https://doi.org/10.1007/978-3-319-73255-8_31-2

Park, D. G., Martin, M. H. E., Ober, C. K., Burlitch, J. M., Cavin, O. B., Porter, W. D., & Hubbard, C. R. (1994). Crystallization of Precursors to Forsterite and Chromium-Doped Forsterite. Journal of the American Ceramic Society, 77(1), 33–40. https://doi.org/10.1111/j.1151-2916.1994.tb06954.x

Parsonage, E., Tirrell, M., Watanabe, H., & Nuzzo, R. G. (1991). Adsorption of poly(2-vinylpyridine)-poly (styrene) block copolymers from toluene solutions. Macromolecules, 24(8), 1987–1995. https://doi.org/10.1021/ma00008a041

Qiu, J., & Matyjaszewski, K. (1997). Metal complexes in controlled radical polymerization. Acta Polymerica, 48(5–6), 169–180. https://doi.org/10.1002/actp.1997.010480501

Schork, F. J., Luo, Y., Smulders, W., Russum, J. P., Butté, A., & Fontenot, K. (2005). Miniemulsion Polymerization. In M. Okubo (Ed.), Polymer Particles: -/- (pp. 129–255). Springer. https://doi.org/10.1007/b100115

Seah, M. P. (1980). The quantitative analysis of surfaces by XPS: A review. Surface and Interface Analysis, 2(6), 222–239. https://doi.org/10.1002/sia.740020607

Sha, J., Jung, B., Thompson, M. O., Ober, C. K., Chandhok, M., & Younkin, T. R. (2009). Submillisecond post-exposure bake of chemically amplified resists by CO2 laser spike annealing. Journal of Vacuum Science & Technology B: Microelectronics and Nanometer Structures Processing, Measurement, and Phenomena, 27(6), 3020–3024.

Silicon | Periodic Table—US. (2024). https://www.thermofisher.com/us/en/home/materials-science/learning-center/periodic-table/metalloid/silicon.html

Song, Y. C., Zhao, Y., Feng, C. X., & Lu, Y. (1994). Synthesis and pyrolysis of polysilazane as the precursor of Si3N4/SiC ceramic. Journal of Materials Science, 29(21), 5745–5756.

Stöber, W., Fink, A., & Bohn, E. (1968). Controlled growth of monodisperse silica spheres in the micron size range. Journal of Colloid and Interface Science, 26(1), 62–69.

Sweat, D. P., Kim, M., Yu, X., & Gopalan, P. (2013). A Single-Component Inimer Containing Cross-Linkable Ultrathin Polymer Coating for Dense Polymer Brush Growth. Langmuir, 29(11), 3805–3812. https://doi.org/10.1021/la305060z

Szczepaniak, G., Fu, L., Jafari, H., Kapil, K., & Matyjaszewski, K. (2021). Making ATRP More Practical: Oxygen Tolerance. Accounts of Chemical Research, 54(7), 1779–1790. https://doi.org/10.1021/acs.accounts.1c00032

Tait, W. R. T., Thedford, R. P., Chapman, D. V., Yu, F., Freidl, J. W., Sablina, E. S., Batsimm, G. M., & Wiesner, U. B. (2021). One-Pot Structure Direction of Large-Pore Co-Continuous Carbon Monoliths from Ultralarge Linear Diblock Copolymers. Chemistry of Materials, 33(19), 7731–7742. https://doi.org/10.1021/acs.chemmater.1c01987

Teper, P., Chojniak-Gronek, J., Hercog, A., Oleszko-Torbus, N., Płaza, G., Kubacki, J., Balin, K., Kowalczuk, A., & Mendrek, B. (2020). Nanolayers of poly (N, N′-dimethylaminoethyl methacrylate) with a star topology and their antibacterial activity. Polymers, 12(1), 230.

Vaahs, T., Brück, M., & Böcker, W. D. G. (1992). Polymer-derived silicon nitride and silicon carbonitride fibers. Advanced Materials, 4(3), 224–226. https://doi.org/10.1002/adma.19920040314

Verbeek, W. (1974). Production of shaped articles of homogeneous mixtures of silicon carbide and nitride (United States Patent No. US3853567A). https://patents.google.com/patent/US3853567A/en

Wang, J.-S., & Matyjaszewski, K. (1995). Controlled/"living" radical polymerization. Atom transfer radical polymerization in the presence of transition-metal complexes. Journal of the American Chemical Society, 117(20), 5614–5615. https://doi.org/10.1021/ja00125a035

Weyer, D. E. (1963). Method of preparing ceramic-like articles (United States Patent No. US3090691A). https://patents.google.com/patent/US3090691A/en

Yajima, S., Hayashi, J., Omori, M., & Okamura, K. (1976). Development of a silicon carbide fibre with high tensile strength. Nature, 261(5562), 683–685. https://doi.org/10.1038/261683a0

Yamada, B. (2015). Free-Radical Addition Polymerization (Fundamental). In S. Kobayashi & K. Müllen (Eds.), Encyclopedia of Polymeric Nanomaterials (pp. 797–810). Springer. https://doi.org/10.1007/978-3-642-29648-2_183

Yan, X., Xu, T., Chen, G., Yang, S., Liu, H., & Xue, Q. (2004). Preparation and characterization of electrochemically deposited carbon nitride films on silicon substrate. Journal of Physics D: Applied Physics, 37(6), 907.

Yu, S. H., Riman, R. E., Danforth, S. C., & Leung, R. Y. (1995). Pyrolysis of Titanium-Metal-Filled Poly(siloxane) Preceramic Polymers: Effect of Atmosphere on Pyrolysis Product

Chemistry. Journal of the American Ceramic Society, 78(7), 1818–1824. https://doi.org/10.1111/j.1151-2916.1995.tb08894.x

Yu, Z., Li, F., & Zhu, Q. (2022). Single-source-precursor synthesis and phase evolution of NbC–SiC–C ceramic nanocomposites with core−shell structured NbC@C and SiC@C nanoparticles. Advanced Powder Materials, 1(1), 100009. https://doi.org/10.1016/j.apmate.2021.09.009

Yuan, C., Käfer, F., & Ober, C. K. (2022). Polymer-Grafted Nanoparticles (PGNs) with Adjustable Graft-Density and Interparticle Hydrogen Bonding Interaction. Macromolecular Rapid Communications, 43(12), 2100629. https://doi.org/10.1002/marc.202100629

Zdyrko, B., & Luzinov, I. (2011). Polymer Brushes by the "Grafting to" Method. Macromolecular Rapid Communications, 32(12), 859–869. https://doi.org/10.1002/marc.201100162

Zhang, S., & Zhao, D. (2012). Aerospace Materials Handbook. CRC Press.

Zhang, X., Chen, Y., & Hu, J. (2018). Recent advances in the development of aerospace materials. Progress in Aerospace Sciences, 97, 22–34. https://doi.org/10.1016/j.paerosci.2018.01.001

Zhao, B., & Brittain, W. J. (2000a). Polymer brushes: Surface-immobilized macromolecules. Progress in Polymer Science, 25(5), 677–710. https://doi.org/10.1016/S0079-6700(00)00012-5

Zhao, B., & Brittain, W. J. (2000b). Polymer brushes: Surface-immobilized macromolecules. Progress in Polymer Science, 25(5), 677–710. https://doi.org/10.1016/S0079-6700(00)00012-